CZECH TECHNICAL UNIVERSITY
IN PRAGUE

Faculty of Nuclear Sciences and Physical Engineering

Department of Physics

Diploma Thesis

Production of J/ψ meson in U+U collisions at the STAR Experiment

Author: Ota Kukral

Supervisor: RNDr. Petr Chaloupka, Ph.D.

Prague, 2014

ČESKÉ VYSOKÉ UČENÍ TECHNICKÉ
V PRAZE

Fakulta Jaderná a Fyzikálně Inženýrská

Katedra Fyziky

Diplomová práce

Produkce J/ψ ve srážkách U+U na experimentu STAR

Autor: Ota Kukral

Vedoucí práce: RNDr. Petr Chaloupka, Ph.D.

Praha, 2014

Vložit zadání práce

Prohlášení

Prohlašuji, že jsem svou diplomovou práci vypracoval samostatně a použil jsem pouze podklady uvedené v přiloženém seznamu.

Nemám závažný důvod proti užití tohoto školního díla ve smyslu § 60 Zákona č.121/2000 Sb., o právu autorském, o právech souvisejících s právem autorským a o změně některých zákonů (autorský zákon).

V Praze dne 21. července 2014 .....

Ota Kukral

Acknowledgements

I am deeply grateful to my supervisor RNDr. Petr Chaloupka, Ph.D. for his persevering help with this analysis. I appreciate his advices, his cooperation and also his effort to motivate me.

I am also very thankful to Mgr. Jaroslav Bielčík, Ph.D. for his continuous support and guidance as well as for his consultations.

Title: **Production of J/psi meson in U+U collisions at the STAR experiment**

Author: Ota Kukral

Branch of study: Experimental Nuclear and Particle Physics

Project: Diploma Thesis

Supervisor: RNDr. Petr Chaloupka, Ph.D.
Department of Physics, FNSPE, CTU in Prague

Abstract: A new state of strongly interacting matter called Quark-Gluon Plasma (QGP) is created in high energy collisions of heavy nuclei. Suppression of heavy quarkonia states in QGP is predicted to be a sensitive indicator of the temperature of the created system. Unfortunately, it is complicated to dissentangle this suppression from other competing effects. Collisions of various heavy-ion systems can help us to understand different sources of quarkonia modification. This work presents the measurement of J/ψ invariant yield and nuclear modification factor in U+U collisions via dielectron decay channel. The data were taken by STAR experiment in 2012.

Keywords: J/ψ, nuclear modification factor, uranium, heavy-ion collisions, quarkonia, QGP, STAR, RHIC

Název práce: **Produkce J/psi ve srážkách U+U na experimentu STAR**

Autor: Ota Kukral

Vedoucí práce: RNDr. Petr Chaloupka, Ph.D.
Katedra fyziky, FJFI, ČVUT v Praze

Abstrakt: Při vysokoenergetických srážkách těžkých iontu vzniká nový stav silně interagujicí hmoty nazývaný kvark-gluonové plazma (QGP). Potlačení produkce těžkých kvarkonií uvnitř této hmoty je považováno za citlivý ukazatel dosažené teploty. Bohužel, pozorování tohoto potlačení je komplikováno přítomností jiných konkurenčních jevů. Pro rozlišení jejich vlivu na modifikaci produkce kvarkonií je třeba studovat srážky různých systémů. V této práci jsou prezentovány výsledky měření invariantního výtěžku a jaderného modifikačního faktoru J/ψ ve srážkách uranu. K tomuto měření byl využit dielektronový rozpadový kanál. Použitá data byla nabrána experimentem STAR v roce 2012.

Klíčová slova: J/ψ, jaderný modifikační faktor, uran, srážky těžkých iontů, kvarkonia, QGP, STAR, RHIC

Contents

Introduction

A new state of QCD matter is created in high energy heavy-ion collisions. This matter is called quark-gluon plasma. It is an unusual state of matter where quarks and gluons, which are normally bound to hadrons, are deconfined. Nowadays, quark-gluon plasma is the object of extensive experimental research primarily at Relativistic Heavy Ion Collider and Large Hadron Collider.

Study of heavy quarkonia (bound $c\bar{c}$ and $b\bar{b}$ states) can improve our understanding of this matter. Their masses are large compared to the temperature of the plasma. Because of that, their production is mostly limited to hard processes that occur in the early stages of the heavy-ion collision. Also, their interaction with hot matter is different from the interactions of light quarks. Thus, quarkonia provide us with a new insight into the properties of the plasma.

This diploma thesis presents the analysis of J/ψ ($c\bar{c}$ state) in U+U collisions at $\sqrt{s_{NN}} = 193$ GeV recorded by the STAR experiment at Relativistic Heavy Ion Collider during year 2012. Purpose of the work was to obtain raw J/ψ signal, utilize data and simulation to correct it for reconstruction efficiencies, extract invariant yield and study J/ψ modification using nuclear modification factor.

The thesis is structured in following manner:
First chapter gives theoretical context of the quarkonia measurement and introduces basic concepts relevant for the analysis. In the second chapter, STAR experiment and its subsystems are described. Chapter three recounts the steps used to obtain raw signal, while chapter four is dedicated to signal corrections. Chapter five presents the results – J/ψ invariant yield and nuclear modification factor. In the appendix, overview of the presentations of the work is given.

Chapter 1

Ultrarelativistic heavy ion collisions

The strong interaction is described in Standard model by Quantum Chromodynamics (QCD). At low temperatures and densities, QCD matter is in hadronic phase, where the behavior of matter is hence driven by the hadronic degrees of freedom. However, at high energy density, QCD predicts that a new state of matter is created [1]. This QCD matter is called Quark-Gluon Plasma (QGP). There, quarks and gluons, normally bound to hadrons, are deconfined. One can draw phase diagram of QCD matter in the plane of temperature T and baryochemical potential μ_B (Fig. 1.1). Between the two phases of matter, phase transition is expected [2],[3]. This transition is expected to be of first order [4] for higher values of μ_B and cross-over in the region of $\mu_B \approx 0$. The two transitions meet at the critical point.

The QCD phase diagram and QGP are a subject of extensive studies, both theoretical and experimental. The most straightforward way to examine QGP properties is via heavy-ion collisions. This is performed in heavy-ion colliders such as the Super Proton Synchrotron (SPS), Relativistic Heavy Ion Collider (RHIC) or Large Hadron Collider (LHC).

There are many remarkable observables and methods employed in experimental QGP studies which will not be discussed here (overview for example in [5]). We will limit ourselves to quarkonium suppression, which is relevant for the analysis presented in this diploma thesis.

1.1 Quarkonia

Quarkonia in a looser sense of word are mesons consisting of quark and same flavor antiquark pair, however in this work we will use the term in a stricter

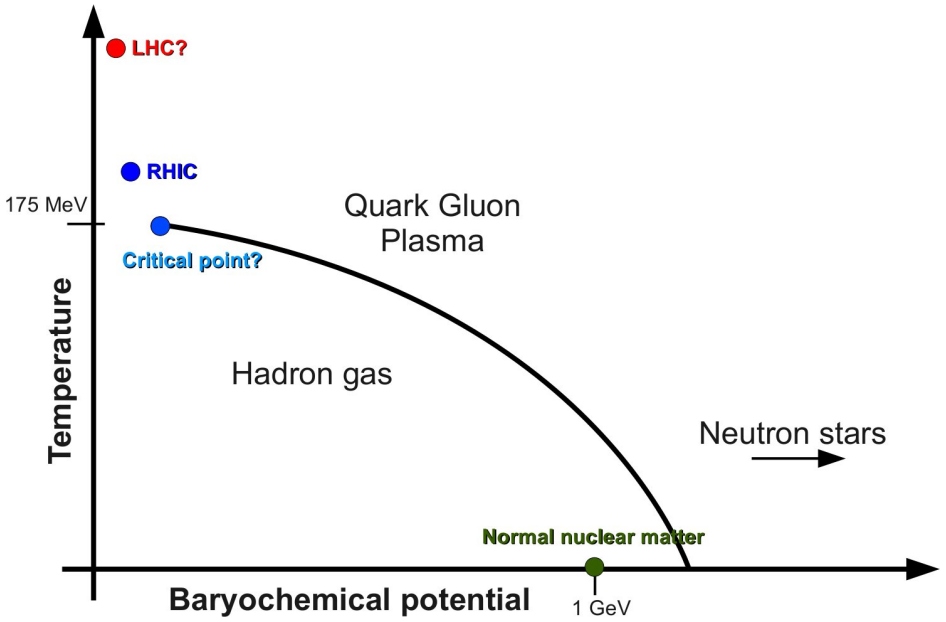

Figure 1.1: Phase diagram of QCD matter in plane of baryochemical potential μ_B and temperature T.

sense of heavy quarkonia, that is only charmonium ($c\bar{c}$) and bottomonium ($b\bar{b}$) are considered.

Several states of quarkonia exist, we will talk about J/ψ, χ_c and ψ', which quark content is $c\bar{c}$, and $\Upsilon(1S)$, $\Upsilon(2S)$, $\Upsilon(3S)$, which are $b\bar{b}$ states.

Importance of heavy quarks for the QGP research comes from the fact that mass of c and b quark is high ($m_c \approx 1.3$ GeV/c^2, $m_b \approx 4.2$ GeVc^2) compared to the temperature of QGP created in heavy-ion collision. The effect is that the production is mostly limited to the hard processes that occur in the early partonic collisions. Moreover, the c and b mass is large compared to typical QCD scale $\Lambda_{\mathrm{QCD}} \approx 200$ MeV as well. This means that the running QCD coupling α_s is small and the production can be described by perturbative QCD. Created quarkonium is then affected by QGP which it passes through. We can learn about QGP by studying this influence.

In order to quantify the effect of QGP on quarkonia, it is useful to introduce nuclear modification factor R_{AB} (Eq. 1.1). It compares the production in A+B collision to p+p production, as p+p is the basic colliding system where QGP is not formed.

$$R_{\mathrm{AB}}(p_{\mathrm{T}}, y) = \frac{\mathrm{d}^2 N^{\mathrm{AB}} / \mathrm{d}p_{\mathrm{T}}\,\mathrm{d}y}{N_{\mathrm{coll}}\,\mathrm{d}^2 N^{\mathrm{pp}} / \mathrm{d}p_{\mathrm{T}}\,\mathrm{d}y}. \tag{1.1}$$

N_{Coll} is the average number of binary collisions in A+B collision, N^{AB} and

N^{pp} are yields in A+B and p+p, p_{T} and y transverse momentum and rapidity. The factor thus gives us the ratio of particle production in A+B to p+p collision. If the production follows binary scaling, the R_{AB} would be 1, number smaller than 1 means suppression, larger than 1 enhancement. R_{AB} for symmetrical collisions is often denoted as R_{AA}.

1.1.1 Quarkonia as QGP thermometer

The quarkonia bounding potential can be nonrelativistically (which is justified by their large mass) described by so called Cornell potential [6],[7]:

$$V(r) = \sigma r - \frac{\alpha}{r}\,. \tag{1.2}$$

The first term corresponds to strong interaction with its confining nature, the second is Coulomb term. By solving this potential in Schrödinger equation, radii r of quarkonia states can be estimated. These are listed together with masses of quarkonia in table 1.1.

	J/ψ	χ_c	ψ'	Υ(1S)	Υ(2S)	Υ(3S)
Mass (GeV/c^2)	3,10	3,53	3,68	9,46	10,02	10,36
Radius (fm)	0,25	0,36	0,45	0,14	0,28	0,39

Table 1.1: Masses and radii of quarkonia states [8], [9].

Already in 1986, Matsui and Satz predicted that charmonia would be suppressed due to in-medium dissociation caused by screening of color charge [10]. This mechanism can be applied to bottomonia as well. This screening is analogical to Debye screening of electromagnetic charge in regular plasma. Potential (1.2) modifies in QGP to:

$$V(r) = -\frac{\alpha}{r}\exp\left[\frac{-r}{r_D(T)}\right]\,. \tag{1.3}$$

The first term in (1.2) disappears as $\sigma \to 0$ in QGP (deconfinement), the second term is modified by the screening. $r_D(T)$ is the characteristical length of the screening. The Debye length is dependent on the temperature of the medium, as temperature increases, so does the strength of the screening – the Debye length decreases. At some point the potential (1.3) does not allow for a bound state – the quarkonium dissolves and we would observe suppression of given state (that is, R_{AA} would be smaller than 1) As the

radii of quarkonia are different for different states, we are able to estimate the temperature of created QGP by measuring which quarkonia are and which are not suppressed. For that we also need to know how the Debye length depends on temperature quantitatively, calculation can be performed on lattice QCD. The exact results of melting temperature are quite model dependent (e.g. [11, 12, 13, 14]), however the main feature is the same: χ_c and ψ' melt already at or below T_c while Υ(1S) survives up to high temperature (Fig. 1.2).

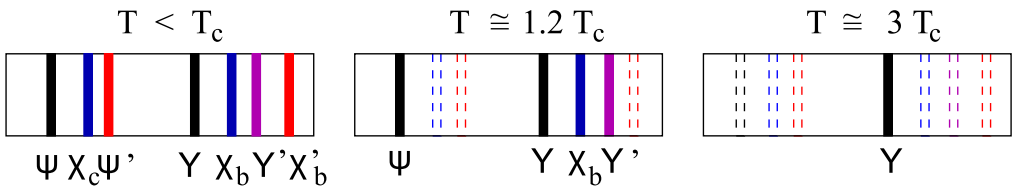

Figure 1.2: Illustration of quarkonia states as a QGP thermometer. Figure from [14].

1.1.2 Challenges

The picture drawn in the previous section is complicated by several competing effects, which dim the interpretation of quarkonia suppression. The most prominent are described in this section.

Sequential melting

Part of the ground quarkonia states is produced by deexcitation of its excited states. This so called feed-down is particularly important for J/ψ. The ratio of J/ψ produced in p+p from χ_c is about $(25 \pm 5)\,\%$ and about $(8.1 \pm 0.3)\,\%$ comes from ψ' [15]. This means that even though the temperature of QGP won't be sufficient to melt J/ψ, the suppression will be observed as melting of excited state will remove the feed-down contribution. Whole situation is depicted in Fig. 1.3.

B meson decays

The other decay contribution which contaminates J/ψ production comes from B meson decays B $\rightarrow$ J/ψ+X. This non–prompt contribution increases from low to high p_{T} and ranges from 10 % to 25 % at STAR in p+p collisions at $\sqrt{s_{NN}} = 200$ GeV [16]. A new STAR detector, Heavy Flavor Tracker

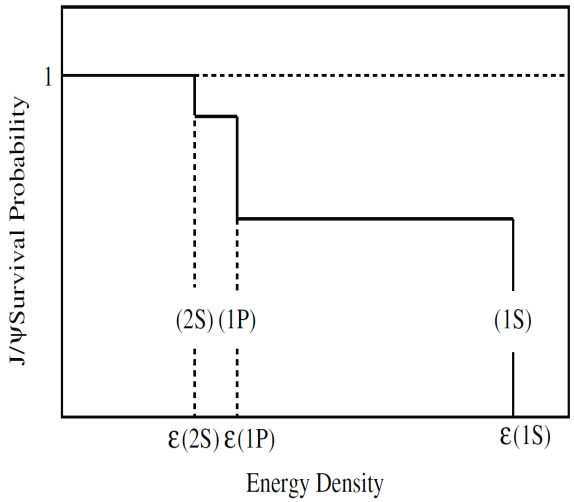

Figure 1.3: Sequential melting of J/ψ. Jumps correspond to the temperatures, where excited state melts. Figure from [9].

(described in chapter 2.) will allow more precise measurement of the B meson decay contribution.

Recombination

There is another production mechanism which plays role in heavy-ion collisions. As quarks are mobile within deconfined QGP, J/ψ can be formed at hadronization from c and $\overline{c}$ quarks which were originally produced in different nucleon-nucleon interactions [17], [18]. Contribution of recombination will increase with number of produced heavy quarks, therefore the effect will be stronger for more central collisions and for higher collision energies – it plays larger role at LHC than at RHIC [19]. Since b quark is produced more scarcely than c quark, the recombination is not so strong for Υ states, which may be then a cleaner probe of QGP.

Cold nuclear matter effects

Not only interaction of J/ψ with hot nuclear matter can affect its observed yields. There are also effects, which are caused by various modifications originating in cold matter. They are called cold nuclear matter (CNM) effects:

- **Nuclear absorption:** Created J/ψ can interact with nucleons along its travel path and dissolve into charmed hadrons such as D mesons or λ_c baryons. The absorption can be described by absorption cross

section σ_{abs}. Studies at SPS and RHIC suggest that this contribution is important and that $\sigma_{\text{abs}} \approx (3-4)$ mb [20],[21]. The suppression in A+A collisions, which can not be attributed to nuclear absorption is sometimes called anomalous suppression.

- **Modification to nuclear parton distribution functions (nPDF):** Parton distribution functions are modified in nucleons in respect to their form in free protons [22],[23]. There are the regions depending on parton momentum fraction x: At low momentum fraction ($x \lesssim 0.02$), the ratio of nuclear PDF to proton PDF is less than 1 – shadowing region. At intermediate fraction ($0.02 \lesssim x \lesssim 0.1$) the ratio is larger than 1 – antishadowing, while for larger fractions it is smaller than 1 again – EMC region.

There can be other CNM effects (e.g. effect of quasi-elastic initial parton scattering [24]). They can be studied in p+A (d+Au) interactions, where QGP is not created, however CNM effects are present.

1.1.3 J/ψ nuclear modification at STAR

STAR has measured J/ψ in p+p, d+Au, Au+Au and Cu+Cu collisions at $\sqrt{s_{NN}} = 200$ GeV [25],[26] and Au+Au collisions at $\sqrt{s_{NN}} = 39$ GeV and 62 GeV [27]. Fig. 1.4 shows the nuclear modification factor for d+Au collisions. STAR preliminary points have large error bars, however if we take into account PHENIX points, we can see that $R_{\text{dAu}} \approx 1$ for high p_{T}.

Fig. 1.5 presents dependence of J/ψ R_{AA} on number of participants and thus on centrality (definition in section 1.2) in Au+Au collisions at $\sqrt{s_{NN}} =$ 200 GeV. The results are for all p_{T} and for high p_{T} only. The suppression increases with centrality (R_{AA} decreases) and decreases for high p_{T}. We can see that J/ψ is suppressed in central collisions even for high p_{T}. Since $R_{\text{dAu}} \approx 1$ for high p_{T}, we expect that this suppression does not originate in CNM effects. Data points in the figure are compared to models that include contributions from prompt production and statistical charm quark regeneration [30][31].

Comparison of suppression of high p_{T} J/ψ between collisions with different energy per nucleon pair is interesting as it can be used to further study the suppression pattern. Fig. 1.6 shows the comparison between data from Au+Au collisions at $\sqrt{s_{NN}} = 200$ GeV and from Pb+Pb at $\sqrt{s_{NN}} = 2760$ GeV. High p_{T}J/ψ at LHC collision energy exhibits significantly higher suppression than at RHIC energy. It is important to note that two data sets are not completely comparable – the rapidity range is different and more

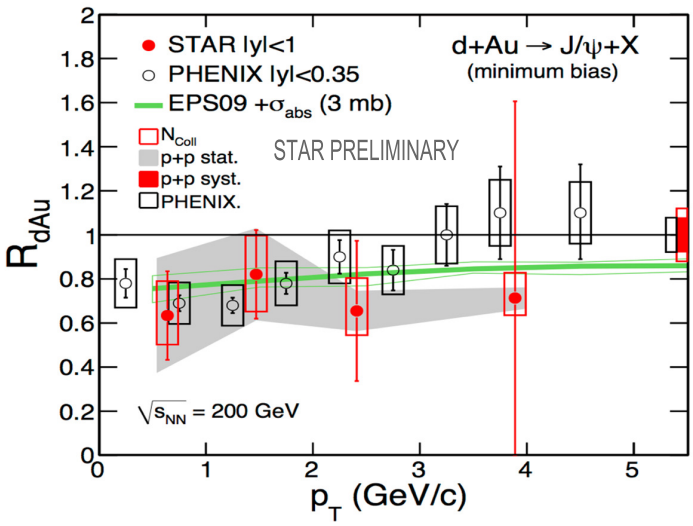

Figure 1.4: J/ψ nuclear modification factor for d+Au at $\sqrt{s_{NN}} = 200$ GeV. Black points are PHENIX data [28], green line EPS09 model including nuclear absorption [29], red points are STAR preliminary.

importantly STAR data show the inclusive J/ψ production while CMS only prompt J/ψ with contribution from B meson decays removed. Nevertheless the overall picture would not change much since prompt and non-prompt J/ψ are similarly suppressed at CMS [33].

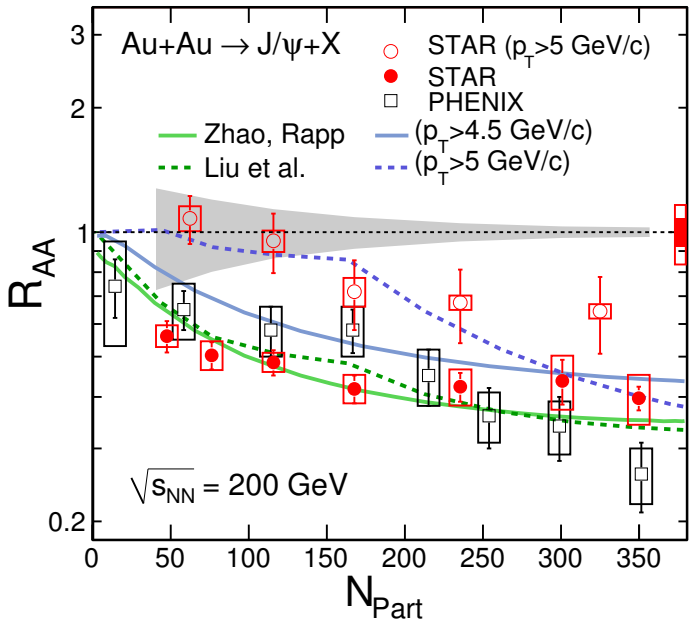

Figure 1.5: Nuclear modification factor R_{AA} for J/ψ in Au+Au at $\sqrt{s_{NN}} =$ 200 GeV. Results are shown for all p_{T} and for high p_{T} only. Lines depict comparison with two models [30][31]. Low p_{T} STAR data from [32], high p_{T} [25]. Figure from [26].

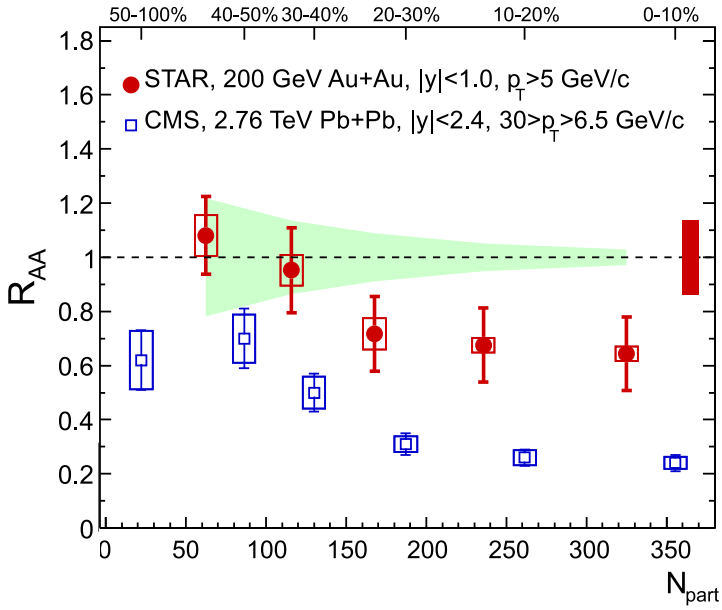

Figure 1.6: Comparison of R_{AA} for high p_{T} J/ψ at STAR [25] and CMS [33].

1.1.4 U+U collisions

Since the interpretation of quarkonia suppression is complicated by an array of competing effects (non-inclusive list in section 1.1.2), it is desirable to study J/ψ in various colliding systems. This analysis was performed on

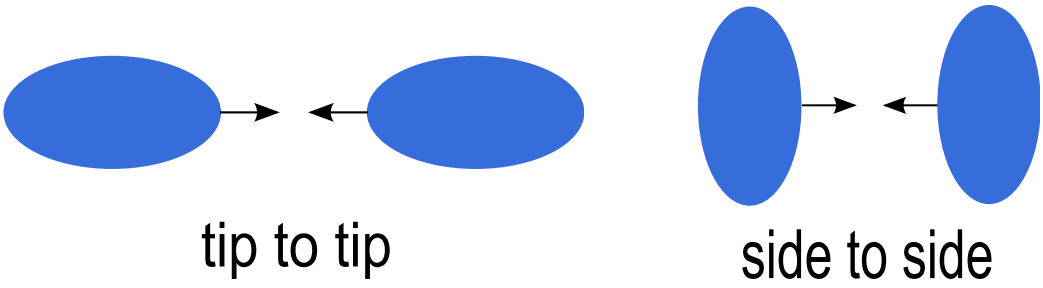

Figure 1.7: Two possible orientations (out of many) of colliding non-spherical nuclei of uranium.

U+U collisions at $\sqrt{s_{NN}} = 193$ GeV which were taken in 2012 by the STAR experiment at RHIC. The uranium is interesting for two reasons:

1. Uranium nuclei are larger than gold nuclei commonly used at STAR. Uranium nucleus has 238 nucleons while gold 197.

2. Uranium is non-spherical, its shape is prolate (like a rugby ball). There exist many possible orientations of incoming nuclei, two most prominent are shown in Fig. 1.7.

This means that the energy density which is achieved in collision is larger than in Au+Au collisions at $\sqrt{s_{NN}} = 200$ GeV by about 20 % when averaged over all possible orientations of incoming uranium nuclei [34],[35] and thus number of tracks in a given event (multiplicity) is larger (Fig. 1.8). Moreover, if we select tip-to-tip collisions, the energy density is even higher. Therefore this systems allows to study J/ψ suppression in a larger system with higher initial energy density.

Nevertheless, the task of selecting tip-to-tip collisions is very challenging from experimental point of view, as there is no control over the alignment of the nuclei. However if we select events with the highest multiplicity, it can be assumed that they originate from tip-to-tip collisions with aligned nuclei centers.

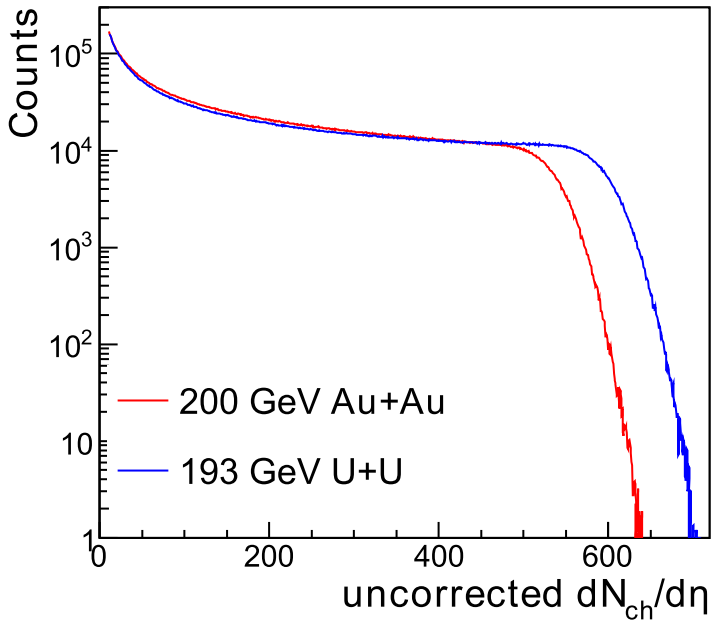

Figure 1.8: Uncorrected multiplicity for Au+Au collisions at $\sqrt{s_{NN}} = 200$ GeV and U+U collisions at $\sqrt{s_{NN}} = 193$ GeV. Figure from [35].

1.2 Observables in heavy-ion collisions

In this section, we will briefly describe basic variables, observables and concepts which are used in the analysis.

1.2.1 Coordinates, rapidity and pseudorapidity

The detector is positioned around interaction point, that is around the point where collisions are supposed to take place. The coordinate system is defined in following way: z axis runs along the direction of beam at the interaction point, y axis is vertical to the ground and x horizontal. p_z, p_y and p_x are then particle momenta along the axes. Transverse momentum is defined as $p_{\mathrm{T}} = \sqrt{p_x^2 + p_y^2}$. The angle in xy plane is called azimuthal angle and denoted ϕ, angle measured from z axis is called polar angle and denoted θ.

It is useful to introduce new variable y called rapidity:

$$y = \frac{1}{2} \ln \left(\frac{E + p_z}{E - p_z} \right),$$

where E is the energy of particle. Dimension of rapidity is 1, the advantage is its additivity for Lorentz boost along the z axis. We also introduce

pseudorapidity η

$$\eta = -\ln(\tan(\theta/2)).$$

If momentum of particle is large ($p \gg m$) relation $y \approx \eta$ holds. Pseudorapidity depends only on the polar angle which is experimentally convenient, as it is much more straightforward to measure the angle than momentum and energy (or mass) of particle.

1.2.2 Impact parameter and centrality

The heavy-ions travel in a beam along the z axis. Their size is ~ 10 fm. Since we can't control their exact position, most impacts are not precisely head-on, but the overlap is only partial. Two groups of nucleons are distinguished: Those that underwent at least one collision – called participants, and the rest – spectators. The overlap is described by so called impact parameter usually denoted b. It is the distance of the centers of nuclei in xy plane, as is depicted in Fig. 1.9. Please note that in case of collisions of non-spherical nuclei, such as uranium, the impact parameter is not sufficient to describe the collision, as for a fixed value of b there can still be infinity of possible orientations of nuclei.

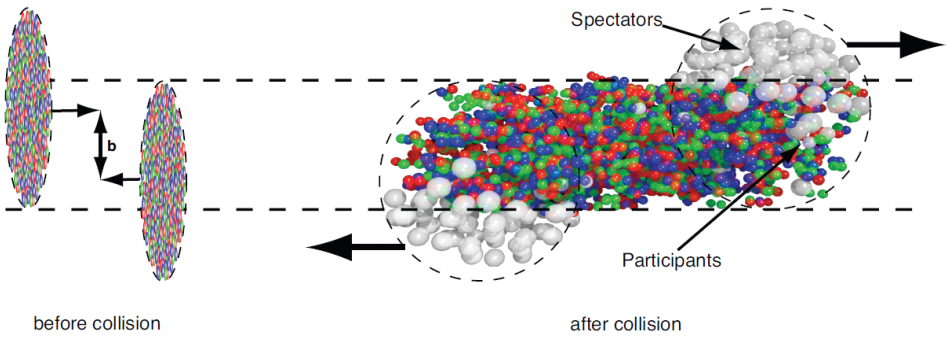

Figure 1.9: Illustration of heavy ion collision. The left drawing shows the situation before the collision, the right after. Figure taken from [36].

The centrality of collision is usually given in percents, where 0 % centrality correspond to the most central collision, while 100 % would be the most peripheral. For spherical nuclei, impact parameter defines the centrality – smaller the parameter, more central the collision is. However, the impact parameter is not measurable experimentally. Two methods of measuring collision centrality are used:

- **Track multiplicity:** More central collision means more participating nucleons and more binary collisions among them, that in turn leads to higher number of tracks observed in a detector – higher multiplicity (Fig. 1.10).

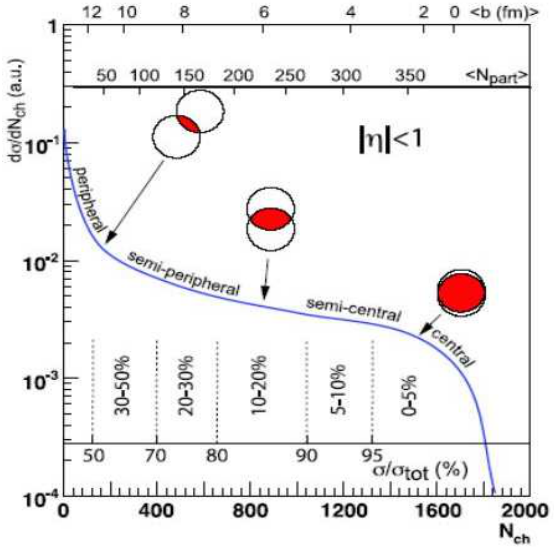

Figure 1.10: Relation between collision centrality and track multiplicity, impact parameter and number of participants N_{part}. Impact parameter, N_{part} and centrality are usually related via Glauber model [37]. Figure from [38].

- **Measurement of spectators**: One can use a detector positioned at same distance in z direction to measure spectator neutrons, while charged fragments are deflected away by magnetic field which keeps the beam on circular trajectory. The number of measured spectators is not directly proportional to the centrality – in the most central collision, number of spectators is 0 (all are participants) while in the most peripheral collision the signal will be also 0 (no free neutrons are kicked out of the nucleus). In STAR, Zero Degree Calorimeters are used for this purpose (description in 2.4).

Chapter 2

STAR experiment

STAR (Solenoid Tracker At RHIC) is a multi-purpose particle detector build to study high energy collisions. It is located in Relativistic Heavy Ion Collider (RHIC) in Brookhaven National Laboratory (BNL) on Long Island, NY, USA, along with PHENIX and two smaller and now decommissioned detectors BRAHMS and PHOBOS. STAR has been used for investigating diverse colliding systems. There have been collisions of p+p, d+Au, Au+Au, Cu+Cu and U+U at various energies.

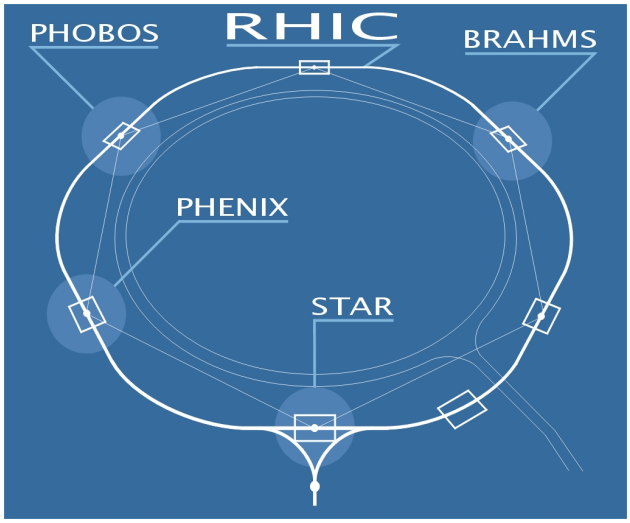

Figure 2.1: Relativistic Heavy Ion Collider with four original experiments. Currently only STAR and PHENIX are in operation.

STAR experiment consist of many different detectors and subsystems that serve different complementary purposes. The main subsystems are shown in Fig. 2.2. Most of the detectors are located in 0.5 T magnetic field generated

by STAR solenoid magnet.

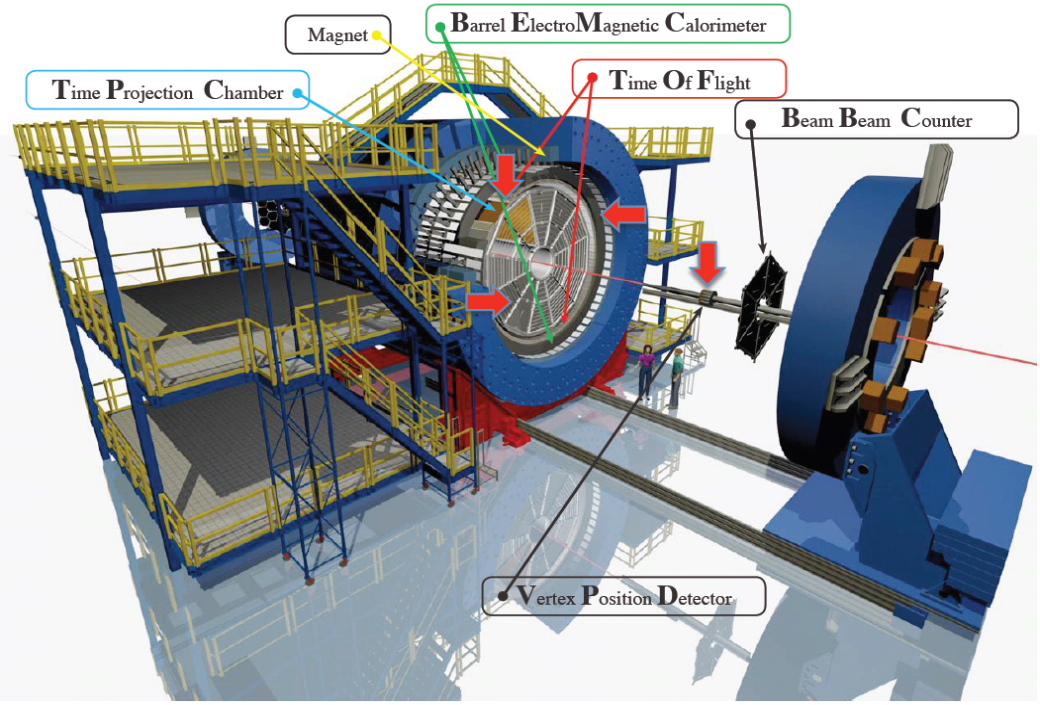

Figure 2.2: Depiction of STAR experiment showing names and positions of the main detectors.

2.1 Time Projection Chamber

Time Projection Chamber (TPC) is the main detector at the STAR experiment. It excels at charged particle tracking and momentum reconstruction, and also at particle identification via specific ionization loss $\mathrm{d}E/\mathrm{d}x$ at midrapidity. This allows for particle identification in a broad range of particle momenta as is illustrated in Fig. 2.3. TPC is a cylinder with length of 420 cm covering 2π in azimuthal angle. Its inner radius is 50 cm, outer radius is 200 cm [39]. Fig. 2.4 is the schematic drawing of the TPC. The detector is filled with a mixture of 10 % of methane and 90 % argon.

2.2 Time of Flight

Another main detector located at STAR is the Time of Flight (TOF) detector. Its main purpose is to improve particle identification by measuring

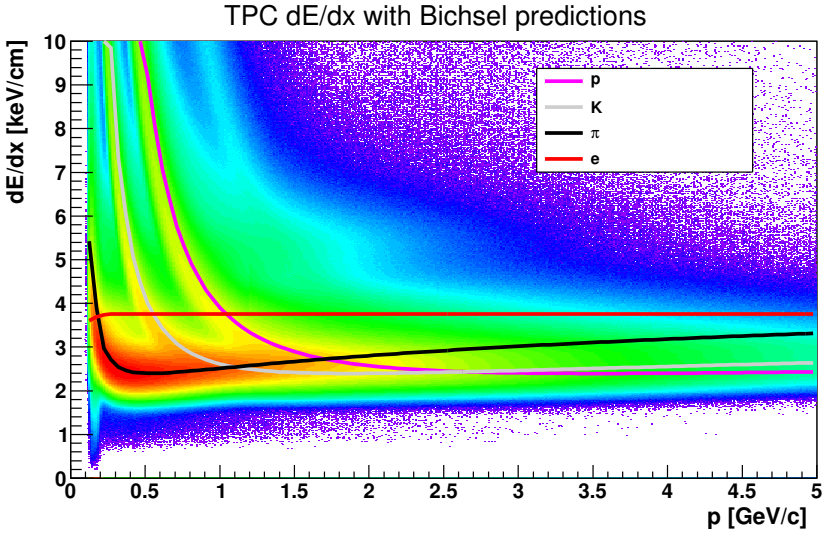

Figure 2.3: Dependence of ionization losses on momentum. Lines show theoretical predictions for various particle species. Picture was obtained from uranium collisions used in this analysis.

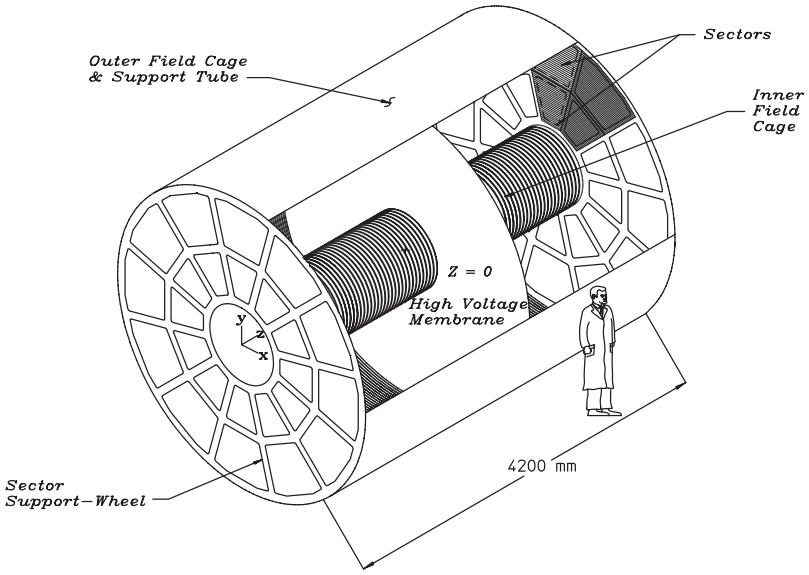

Figure 2.4: Schematic drawing of TPC. Taken from [39].

their velocity β. It is based on Multi-gap Resistive Plate Chamber (MRPC) technology, which has been developed for LHC [40]. In principle, it is a stack

of glass resistive plates with uniform gas gaps. Electric field is applied to the outer surface of the outer plates. When a charged particle goes through the stack, it generates avalanches in the gas gaps. The glass plates are resistive and thus transparent to charge induction – induced signal is the sum of avalanches. The signal read out is provided by an array of copper pads. For the determination of starting time (time of the collision), Vertex Position Detector (described later in this chapter) is used. Since the detector has a very fast timing resolution under 100 ps it is also used for event triggering.

2.3 Barrel Electromagnetic Calorimeter

Barrel Electromagnetic Calorimeter (BEMC) lies outside of TOF also covering 2π in azimuthal angle. It covers pseudorapidity $|\eta| < 1$. BEMC consists of 120 modules, each of which is formed by 40 towers [41]. Each tower spans $\approx 0,05$ in azimuthal angle and 0,05 in pseudorapidity. This means that the tower size differs with different pseudorapidity. Moreover, they are tilted in a way that they point toward interaction point as shown in Fig. 2.5. Towers are composed of 21 layers of lead alternating with 21 layers of scintillators. First 2 layers are read out separately as a preshower detector. There is also a Shower Maximum Detector between 5th and 6th layer, approximately in depth where the shower is the widest. BEMC is used for discrimination of electrons from hadrons. Electrons deposit all of their energy in the calorimeter, while hadrons either do not create a shower or deposit only a fraction of their energy. Therefore E/p ratio for electrons is ≈ 1, while for hadrons it is lower. BEMC is a fast detector, and is thus used for triggering.

2.4 Zero Degree Calorimeters

Zero Degree Calorimeters (ZDCs) are two hadron calorimeters positioned approximately 18 meters from interaction point on both sides of the detector. Their purpose is to detect spectator neutrons emitted within the cone along beam axis after the collision. They are placed directly in direction of the beam coming from the opposite side of the interaction point. The beam and charged spectators are deflected away by dipole magnet while neutrons continue their flight in straight line. Position so close to the beam trajectory limits ZDCs' width to 10 cm. Coincidence of a ZDC signal in the both beam directions is a minimum bias selection of heavy ion collision. This allows its use as a trigger [42].

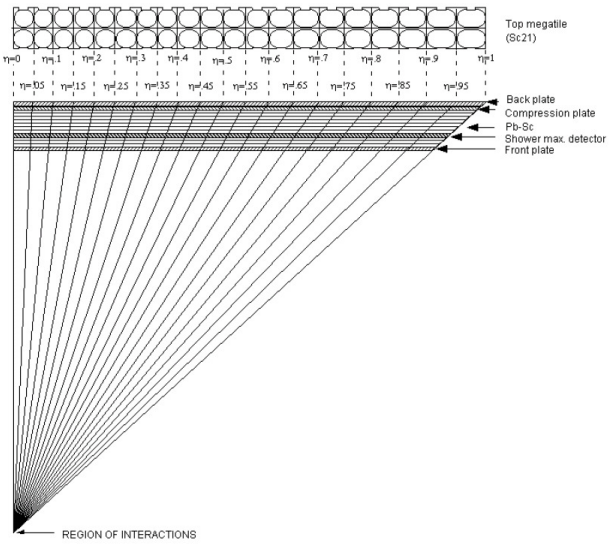

Figure 2.5: Schematic drawing of BEMC illustrating projective nature of towers. Taken from [41].

2.5 Vertex Position Detector

Vertex Position Detector (VPD) consist of two plastic scintillators placed in the equal distance from the experiment center close to the beam axis. In high energy heavy ion collisions, large numbers of very forward and high energy photons are produced which travel from the collisions vertex as a prompt pulse. By measuring time at which these pulses reach two equally spaced detectors we can extract the primary vertex z position. Another use of VPD is to provide starting time for TOF measurement and due to its fast response it is used for triggering as well [43].

2.6 New detectors

There are two new detectors at STAR, Muon Telescope Detector (MTD) and Heavy Flavor Tracker (HFT). These were not available during year 2012 and thus were not used in this analysis, however they are relevant for any future J/ψ analysis performed by STAR and hence are discussed in this section.

2.6.1 Muon Telescope Detector

Muon Telescope Detector (MTD) is a new muon detector located at midrapidity $|\eta| < 0.5$ as the outermost detector, at distance of 400 cm outside of

the magnet flux return iron bars (Fig. 2.6). The detector allows to study J/ψ in its dimuon decay channel J/$\psi \rightarrow \mu^+\mu^-$ and will increase the precision of measurement of modification factor (Fig. 2.7).

Figure 2.6: View of MTD detector and its position on the outside of the STAR detector. Each row consists of 5 MTD modules (not all 5 are visible in the picture), at the bottom of the detector some rows consist of less modules due to space constraints.

The design of the detector is based on multi-gap resistive plate chambers with long readout in 122 modules with total of 1464 read-out strips [46],[45]. Each module consist of two stacks of glass plates forming a total of 10 uniform gas gaps. MTD also utilizes precise timing of TOF system and will allow us to trigger for J/ψ in central heavy-ion collisions. 63 % of the detector was installed for 2013 run, Fig. 2.8 shows the first J/ψ peak from p+p collisions. The whole detector was installed for 2014 run.

2.6.2 Heavy Flavor Tracker

Heavy Flavor Tracker (HFT) is the new detector offering precise pointing resolution of the tracks to primary vertex [47]. Thus the detector allows to study displaced vertices. Its main aim is to enhance capability of STAR to measure heavy flavor by allowing direct topological reconstruction of open charm (D and B mesons) as well as to enable measurement of λ_c baryon.

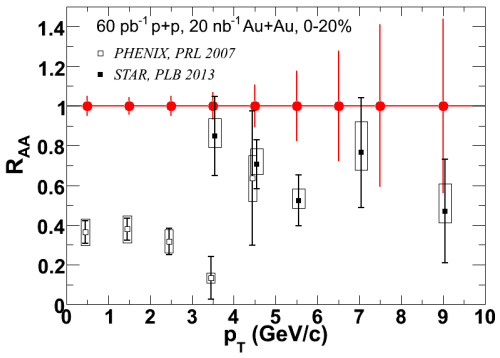

Figure 2.7: Red points illustrate precision of measurement of J/ψ nuclear modification factor for central collisions, which will be achieved by MTD. Black data points are current STAR and PHENIX measurements [25],[44]. Figure from [45].

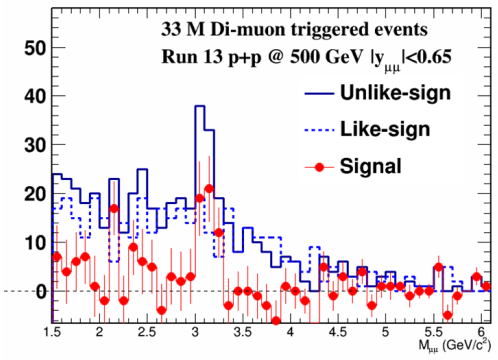

Figure 2.8: First preliminary J/ψ signal extracted from p+p data from year 2013, when MTD was partially installed. Figure from [45].

In the area of J/ψ measurement, HFT will be used to separate prompt J/ψ (directly produced) from non-prompt (from B meson decay) and thus improve our understanding of J/ψ production and suppression mechanisms. Fig. 2.9 displays this separation ability of HFT.

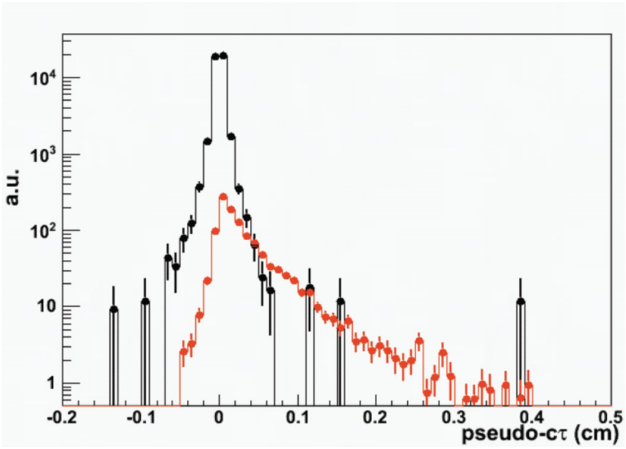

Figure 2.9: Simulation of separation of prompt J/ψ production (black) from non-prompt (red) using HFT. Figure from [47].

HFT is the STAR innermost detector located right around the beam pipe [48]. The detector is in fact an arrangement of four detectors, from the inside

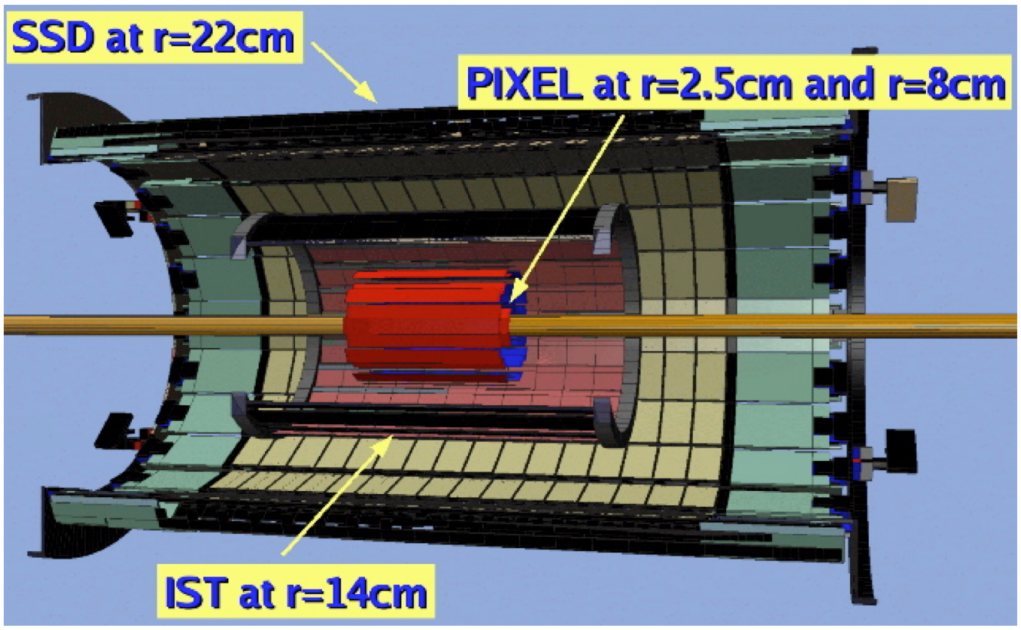

Figure 2.10: Illustration of four layers of HFT and their position in the proximity of the beam pipe. Figure from [48].

there are two layers of Pixel detector at the distance of 2.5 cm and 8 cm from the center of beam, then there is the Intermediate Silicon Tracker (IST) at 14 cm and the Silicon Strip Detector (SSD) is the outermost part of HFT located at 22 cm (Fig. 2.10). The tracks from TPC are matched to outer layers of HFT, which in turn point to inner layers with higher precision. There is some redundancy since a track does not have to leave a signal in all layers. In this way, final pointing precision of ≈ 30 μm is achieved. Another important factor in the detector design was demand of the lowest possible material increase. The achieved radiation thickness is about 0.4 % X_0 for each layer of the Pixel, 1.5 % X_0 for IST and 1.0 % X_0 for SSD. HFT was installed for high luminosity Au+Au run in 2014.

Chapter 3

J/ψ analysis

This chapter describes extraction of J/ψ signal. The analysis builds on the work done as a part of my research project [49].

3.1 Data sample

This analysis was performed using minimum bias U+U collisions at $\sqrt{s_{NN}} =$ 193 GeV taken in 2012 by the STAR experiment at RHIC. The minimum bias events were selected using VPD and ZDC trigger. The total number of events with any accepted trigger was 377 millions. The distribution of uncorrected multiplicity is shown in Fig. 3.1.

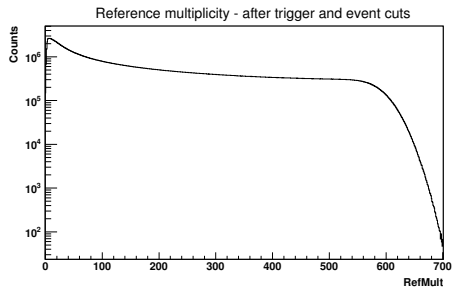

Figure 3.1: Distribution of uncorrected multiplicity for minimum bias triggers.

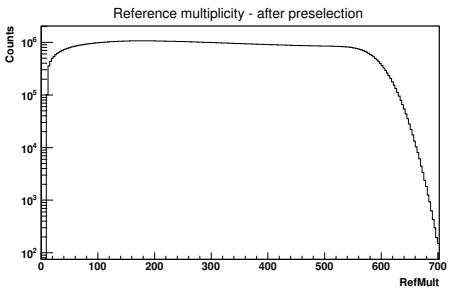

Figure 3.2: Distribution of uncorrected multiplicity after preselection, where only events with a suitable electron candidate are saved.

3.1.1 Preselection

In STAR, data used for the analysis are stored in the data files called MuDST. However, these files are too large and contain much information unnecessary for this particular analysis. It is a common practice to extract only information relevant for particular analysis from these files and store it in smaller files called PicoDST. Since the storage space is limited, we stored only events with at least one suitable electron candidate to further reduce amount of data to be saved. After the preselection, around 180 millions of events is saved. All cuts used in selecting suitable events were weaker than cuts used later in the actual analysis, therefore the results are not affected by the preselection. The cuts are described in more detail in following sections. Fig. 3.2 shows the distribution of uncorrected multiplicity after the preselection, the increase in high multiplicity region is caused by higher probability of finding electron candidate in those events.

3.2 Event cuts

First, bad or questionable runs are removed based on basic quality assurance. Then, events are required to fulfill a few cuts to ensure their good quality. The events position has to be in the middle of the detector, its z distance (along the beam axis) from the center of the detector has to be smaller then 30 cm. Fig. 3.3 shows the distribution of the primary vertex position. Difference between reconstructed z position of the primary vertex by TPC and VPD has to be smaller then 3 cm in order to remove false pile-up events, the distribution is shown in Fig. 3.4.

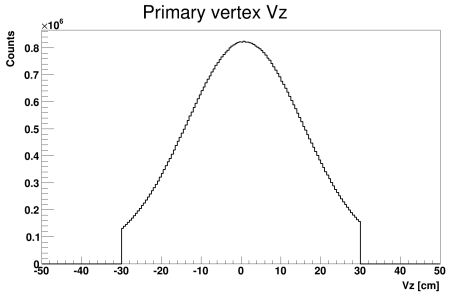

Figure 3.3: Distribution of primary vertex position

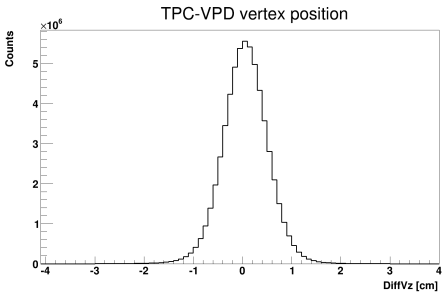

Figure 3.4: Difference between primary vertex z position as reconstructed by TPC and VPD.

Reference multiplicity of the event has to be larger than 10, this corresponds to 0-80 % of most central collisions. Centrality is discussed in more

detail in following section.

3.3 Centrality selection

In the STAR experiment we select centrality of the event from its measured multiplicity. The relation between the observed number of particles and the unobservable impact parameter is deduced from Monte Carlo Glauber model [37]. Centrality regions are based on preliminary Matsui's work [50]. The multiplicity boundaries are summarized in Tab. 3.1:

% centrality	Multiplicity
5 %	> 535
10 %	> 466
15 %	> 399
20 %	> 339
25 %	> 283
30 %	> 233
35 %	> 189
40 %	> 151
45 %	> 118
50 %	> 91
55 %	> 68
60 %	> 50
65 %	> 35
70 %	> 24
75 %	> 16
80 %	> 10

Table 3.1: Multiplicity boundaries used in centrality definition.

Due to trigger inefficiencies for events with very low multiplicity, only events with multiplicity larger then 10 are considered thus limiting the analysis to 0-80 % of most central collisions.

3.4 Trajectory cuts

There are several conditions that have to be fulfilled for a particle trajectory to be used. Number of fitted TPC hits has to be larger than 19 and ratio of fitted hits to maximum possible has to be larger than 0.51. This cut ensures that we do not use tracks that would be obtained from a single track split artificially into two. Only primary trajectories are used. Each track is required to have the distance of closest approach (DCA) of trajectory to the primary vertex smaller than 3 cm. Pseudorapidity η of the trajectories has to be between -1 and 1. The mentioned distributions with applied cut values are shown in Fig. 3.5 and 3.6.

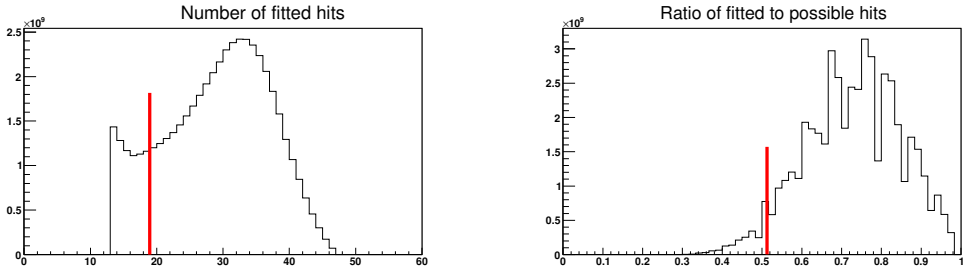

Figure 3.5: Left: Number of fitted hits in TPC. Right: Ratio of fitted to maximum possible hits in TPC. Red lines show cuts used.

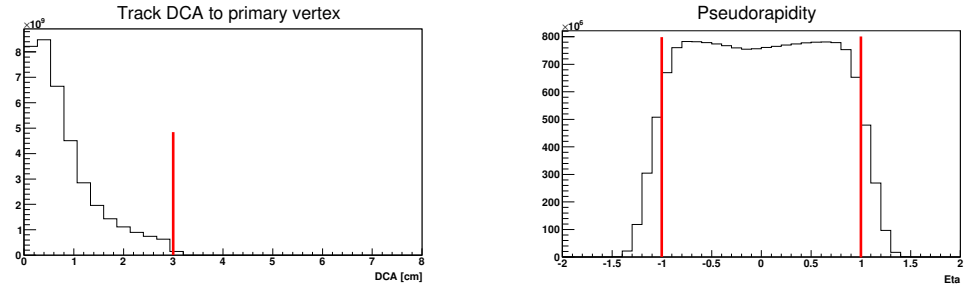

Figure 3.6: Left: Distance of closest approach of trajectory to primary vertex. Right: Pseudorapidity of primary tracks. Red lines show cuts used.

3.5 Electron selection

From primary trajectories which passed the trajectory cut electrons are selected in order to reconstruct J/ψ via its dielectron decay channel. Data

from TPC, TOF and BEMC are used for the electron identification. The detectors are described in chapter 2.

3.5.1 TPC

Particles can be identified by their specific ionization loss pattern in TPC. This ionization energy loss is expressed in $n\sigma$ units. For a given particle species and momentum, distribution of $\log(\mathrm{d}E/\,\mathrm{d}x)$ is supposed to have a Gaussian shape with a mean described by Bichsel function $B = f(p/m)$ and variance given by resolution of $\mathrm{d}E/\,\mathrm{d}x = \sigma$. Then $n\sigma$ is the distance from this mean expressed as a number of standard deviations:

$$n\sigma = \frac{\log((\mathrm{d}E/\,\mathrm{d}x)/B)}{\sigma}. \tag{3.1}$$

In an ideal case $n\sigma$ has a normal distribution – mean is 0 and standard deviation is 1. In our analysis $n\sigma_e$ for electrons and $n\sigma_\pi$ for pions is used.

For electrons, $n\sigma_e$ is required to be $-1.5 < n\sigma_e < 2.0$. Fig. 3.7 shows the $n\sigma_e$ versus particle momentum after TOF and BEMC cuts have been applied. The figure also illustrates why asymmetric cut is used – the hadron contamination is larger from particles with lower $\mathrm{d}E/\mathrm{d}x$.

3.5.2 TOF

TOF detector is used to measure particle velocity β. Due to their low mass, electrons have $\beta \approx 1$ for the whole range of considered momenta. We require $0.97 < 1/\beta < 1.025$, the asymmetry of the cut is based on the relation $\beta_{\mathrm{electron}} > \beta_{\mathrm{hadron}}$ for particles with the same momentum. For a particle to have a valid TOF signal, $|y_{\mathrm{local}}| < 1.8$ cm is demanded, where y_{local} is distance of the track projection and the center of TOF pad. This condition ensures removal of false matches in the detector.

Particles with $p < 1.4$ GeV/c have to fulfill the TOF cut strictly. For particles with $p > 1.4$ GeV/c the advantage of using TOF is lower, since also pions have β close to 1 and $\mathrm{d}E/\mathrm{d}x$ bands do not overlap in that momentum region. Moreover, BEMC is used for $p > 1.4$ GeV/c. Therefore the cut is used for particles with $p > 1.4$ GeV/c only if they have a valid TOF signal. This prevents unnecessary diminishing of electron identification efficiency. Fig. 3.8 shows the TOF cut for particles that have already fulfilled TPC and BEMC cuts.

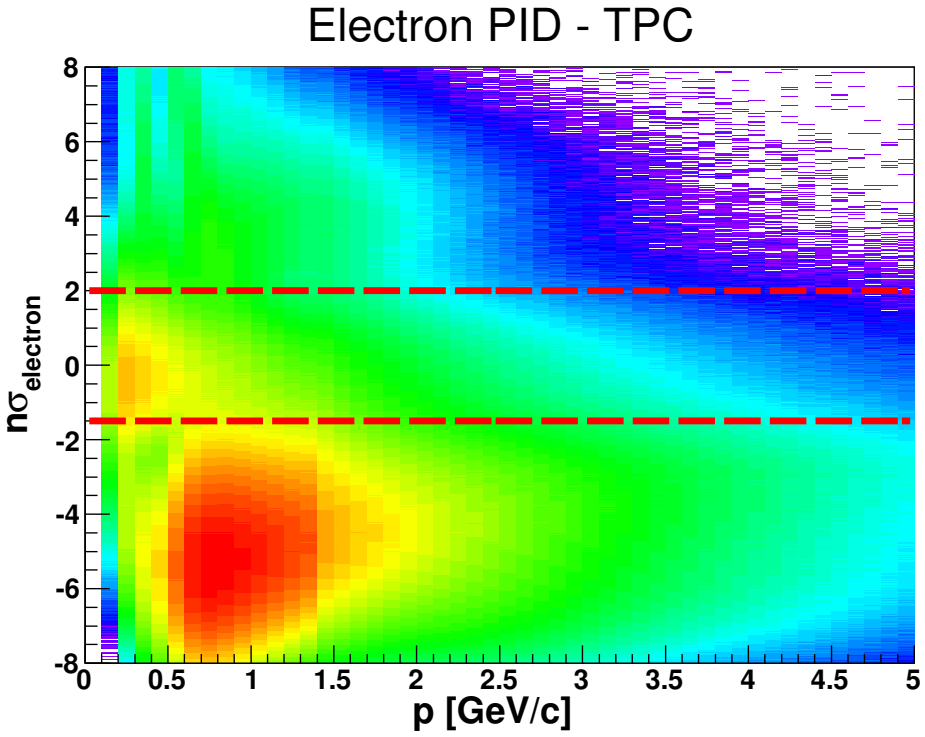

Figure 3.7: $n\sigma_e$ in logarithmic scale for particles which have already passed TOF and BEMC cuts. Red lines show $n\sigma_e$ cut.

3.5.3 BEMC

BEMC is used to obtain an energy E which was deposited in a single tower. Electrons, unlike hadrons, are supposed to deposit all of their energy in the calorimeter, hence having ratio $E/p \approx 1$. This can be used to further suppress hadron contamination in higher p. However, besides calorimeter resolution, there are two other effects which change the electron energy deposited in the calorimeter and thus E/p ratio. First, the electron energy can leak into neighboring towers, especially if the trajectory hits close to an edge of the tower. In this case, the registered E is smaller and E/p smaller than 1. The other effect happens since U+U collisions are high multiplicity events: There can be energy registered in the tower, which comes from other particles hitting the calorimeter nearby. This makes E/p larger than 1.

BEMC cut is used only for particles with $p > 1.4$ GeV/c, where we require $0.5 < E/p < 2$. For particles with $p < 1.4$ GeV/c, TOF is better at distinguishing electrons. $p = 1.4$ GeV/c for the cut change is motivated by similar STAR measurements.

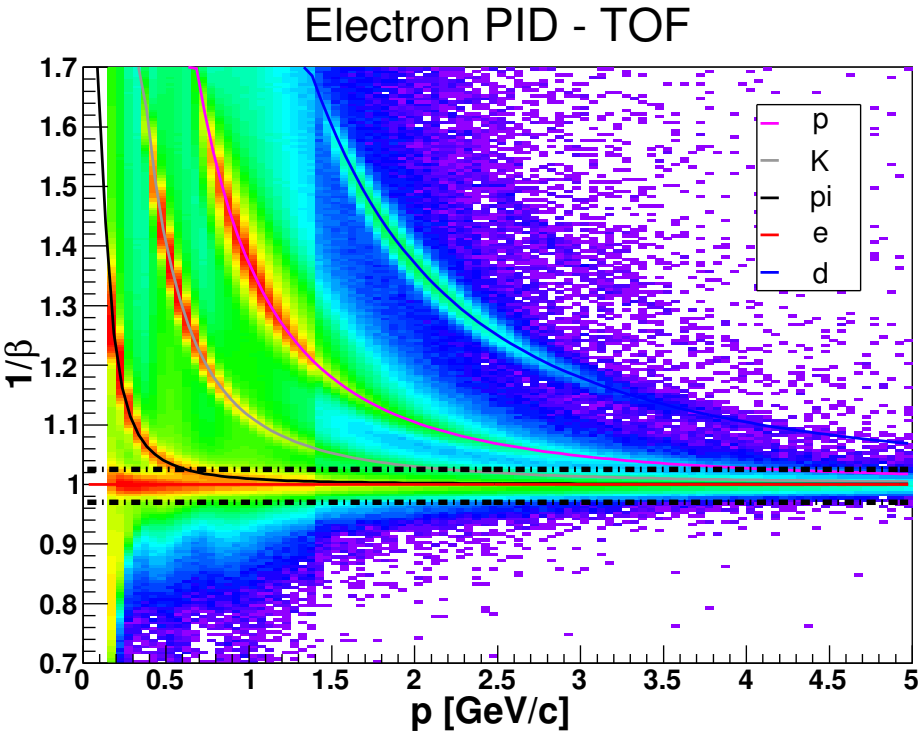

Figure 3.8: $1/\beta$ in logarithmic scale for particles which have already passed TPC and BEMC cuts. Black lines show TOF cut.

3.6 Signal reconstruction

In this work we reconstruct J/ψ via dielectron decay channel $J/\psi \rightarrow e^+e^-$ with branching ratio 5.9 %. Electrons with opposite signs were combined to obtain their invariant mass. If these electron pairs come from J/ψ decay, their invariant mass is equal to the rest mass of J/ψ. There is a large combinatorial background originating from pairs which were combined by chance. Three methods have been used to reconstruct this background:

- **Like–sign method**: Electrons with same charge signs are combined within the same event.
- **Track rotation**: Invariant mass is reconstructed from electrons with unlike signs, where one of them has its momentum vector rotated by 180° in azimuthal angle.
- **Event mixing**: Electrons with opposite signs are combined, but coming from different events, Events used for combining should have similar properties, such as multiplicity and vertex z position.

The best description of combinatorial background was obtained by like–sign method. For this reason it is the method used for all following results.

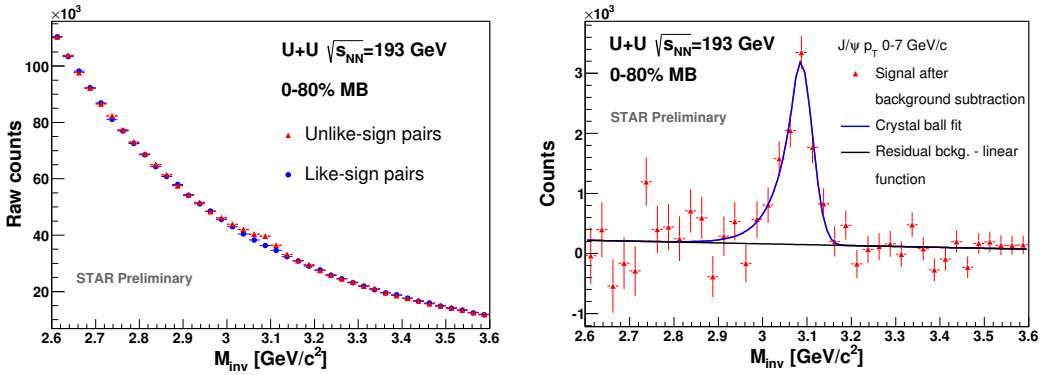

Figure 3.9: Left: Invariant mass of unlike-sign and like-sign electron (positron) pairs in 0-80 % most central U+U collisisons at $\sqrt{s_{NN}} = 193$ GeV. Right: Signal after background subtraction fitted with crystal ball function superimposed on a linear residual background.

Fig. 3.9 shows the invariant mass of unlike and like-sign pairs on the left panel. Right panel displays the signal after invariant mass of like-sign pairs has been subtracted from that of unlike-sign pairs. Even after the subtraction there is still some small background present in the data. This so called residual background was fitted with linear function in the plot, but second order polynomial and exponential function were used for estimating residual background as well. These functions were fitted in 2 mass ranges of (2.6 – 3.6) GeV/c^2 and (2.4 – 3.8) GeV/c^2. The average was then taken as the value of residual background, the difference was used to estimate systematic uncertainty. Crystal ball function [51] was used to fit the actual signal:

$$f_{CB}(m) = \begin{cases} \frac{N}{\sqrt{2\pi}\sigma} \exp\left(-\frac{(m-m_0)^2}{2\sigma^2}\right) & \text{for } \frac{m-m_0}{\sigma} > -\alpha \\ \frac{N}{\sqrt{2\pi}\sigma} \left(\frac{n}{|\alpha|}\right)^2 \exp\left(-\frac{|\alpha|^2}{2}\right) \left(\frac{n}{|\alpha|} - |\alpha| - \frac{m-m_0}{\sigma}\right)^{-n} & \text{for } \frac{m-m_0}{\sigma} \leq -\alpha \end{cases} \tag{3.2}$$

It is a Gaussian with a tail, which accounts for electron radiation losses and also for J$\psi \to \gamma\, e^+e^-$ decay in which we are not able to detect the photon. The crystal ball function has 5 parameters: m_0 for mean, N is normalization constant, σ for width of the peak and n and α for describing the tail.

In order to reduce signal dependency on the fitting procedure, the actual number of J/ψ is obtained by bin counting in mass region of J/ψ, that is (2.9 – 3.2) GeV/c^2, and then subtracting the residual background.

Statistical significance of signal is calculated as

$$Sg = \frac{S}{\sqrt{S + 2B}}, \tag{3.3}$$

where S is number of J/ψ in mass region (2.9-3.2) GeV/c^2 and B is background in the same mass region. We obtained significance of 11 for 0-80 % most central collisions.

3.6.1 Signal p_{T} dependence

We have divided the J/ψ signal into 6 p_{T} bins going from 0 up to 7 GeV/c. Signal after background subtraction with crystal ball + linear function fit is in the first three plots of Fig. 3.10.

Significance of a signal in various p_{T} bins has been calculated according to Eq. 3.3 and varies between 3–7.

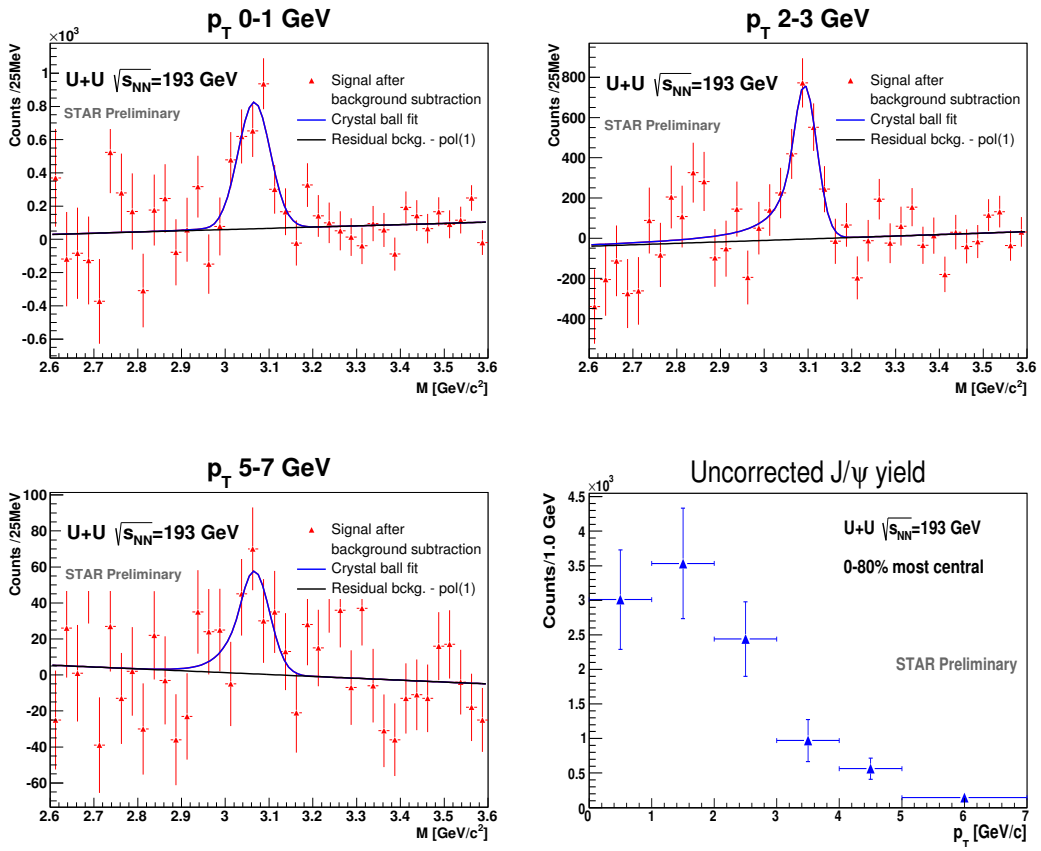

Figure 3.10: First three plots: Signal after background subtraction for several p_T bins. Signal is then fitted with a crystal ball function, linear function is added to fit residual background. Bottom right: J/ψ uncorrected counts as a function of transverse momentum for 0-80 % most central collisions.

3.6.2 Centrality dependence

Study of R_{AA} centrality dependence is important for understanding the origins and mechanisms of J/ψ suppression. Furthermore, selecting very central collisions is the only way how to have some control over orientations of colliding uranium nuclei, as it leads to selecting tip-to-tip collisions.

J/ψ signal has been studied in the 0-10 % most central collisions (Fig. 3.11) and in the peripheral collisions (60-80 %, Fig. 3.12). Raw count in central collisions is higher than in peripheral, however combinatorial background is also much higher. This results in similar significance (calculated as 3.3) in both centralities. Use of centrally triggered data, which were also stored, is planned in order to further improve statistics for most central collisions.

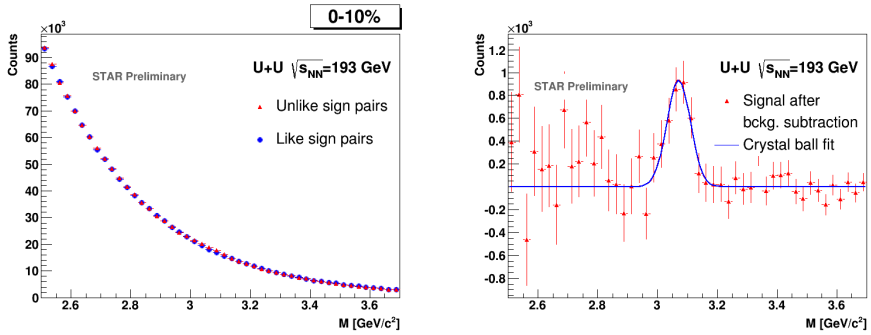

Figure 3.11: Left: Invariant mass of unlike and like-sign pairs for 0-10 % most central collisions. Right: Signal after background subtraction for 0-10 % most central collisions fitted with a crystal ball function.

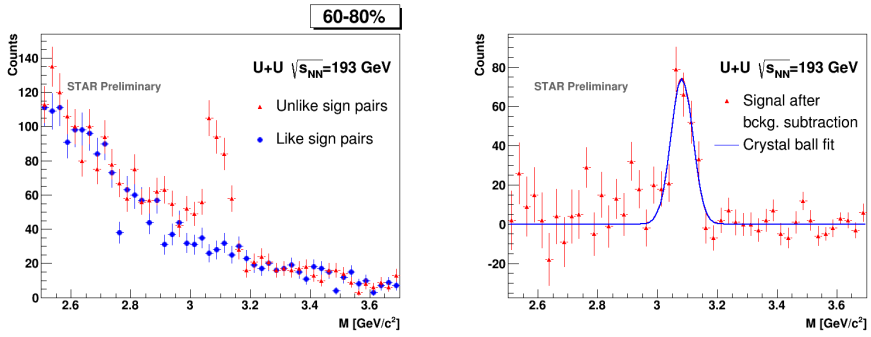

Figure 3.12: Left: Invariant mass of unlike and like-sign pairs for peripheral collisions (60-80 %). Right: Signal after background subtraction for centrality 60-80 %. Signal is fitted with a crystal ball function.

Chapter 4

Signal corrections

The raw signal shown in chapter 3.6 needs to be corrected for all J/ψ that were not reconstructed by our analysis. There are two main groups of corrections. First is detector acceptance – matching efficiency, which is the ratio between particles (e.g. electrons) registered in a given detector and all particles. The other is cut efficiency – the ratio of particles selected by our cut to all registered in the detector.

4.1 Single electron PID efficiency

We have to correct for the cuts used in TPC, TOF and BEMC. The procedure for the signal corrections is following: We define single electron PID efficiency, which includes all corrections from TOF and BEMC for single electrons. It also includes TPC cut efficiency. The single electron PID efficiency is given by formula:

$$\epsilon_{\mathrm{sPID}} = \begin{cases} \epsilon_{\mathrm{dEdx}} \times \epsilon_{\mathrm{BEMCmatch}} \times \epsilon_{\mathrm{BEMCcut}} \times (\epsilon_{\mathrm{TOFmatch}} \times \\ \qquad \times \epsilon_{\mathrm{TOFcut}} + (1 - \epsilon_{\mathrm{TOFmatch}})) & \text{for p: } > 1.4\mathrm{GeV/c} \\ \epsilon_{\mathrm{dEdx}} \times \epsilon_{\mathrm{TOFmatch}} \times \epsilon_{\mathrm{TOFcut}} & \text{for p: } < 1.4\mathrm{GeV/c}. \end{cases} \tag{4.1}$$

ϵ_{dEdx} is TPC cut efficiency, $\epsilon_{\mathrm{BEMCmatch}}$ and $\epsilon_{\mathrm{TOFmatch}}$ is BEMC and TOF matching efficiency and $\epsilon_{\mathrm{BEMCcut}}$ ($\epsilon_{\mathrm{TOFcut}}$) is BEMC (TOF) cut efficiency. The form of the equation for electrons with momentum higher than 1.4 GeV/c is dictated by the two possible ways how a particle can be flagged as an electron: either it has a signal in TOF (with probability $\epsilon_{\mathrm{TOFmatch}}$) and then it has to pass the TOF cut ($\epsilon_{\mathrm{TOFcut}}$) or it does not have a valid TOF signal at all (with probability $(1 - \epsilon_{\mathrm{TOFmatch}})$). This correction is not final, the calculation of the overall reconstruction efficiency is described in section 4.2.

For the extraction of efficiencies from data, following technique is used: We need to obtain a pure electron sample which should be as much as possible without hadron contamination. However, if the efficiency of given detector is studied, the detector can not be used to obtain this sample. This in turn leads to low purity of the sample. In order to improve the purity, only electron positron pairs from photonic electrons (from γ conversion and π^0 and η decays) are used as they are significantly less contaminated. Photonic electrons are selected by cut on invariant mass of the pair, it has to be lower then 12.5 MeV. To reduce hadron contamination even further, one electron from the candidate photonic pair is required to fulfill all detector cuts, and then the other one is saved. The saved electron was selected without the studied detector and is thus unbiased. The downside of the technique is reduced statistics.

If we want to lower remaining hadron contamination, we can use same–sign photonic pairs selected by the same procedure as our electron sample, but this time requiring that the charge sign is the same for both particles in the pair. These electrons describe the combinatorial contribution to the photonic sample and are thus subtracted from it. This technique was used only for determining BEMC cut efficiency.

Following sections explain how individual terms of equation (4.1) are obtained.

4.1.1 TPC

TPC cut efficiency

Electron $n\sigma_{\mathrm{e}}$ (defined by (3.1)) is required to be $-1.5 < n\sigma_e < 2.0$. The cut efficiency is obtained from data. First, photonic electron sample is selected. The electron sample is then divided into momentum bins. In each bin, $n\sigma_e$ distribution of the specific ionization loss $\mathrm{d}E/\mathrm{d}x$ is fitted with two Gaussians, one describing electrons and the other remaining pion contamination. As there is some contribution from merged pion tracks, which distribution is not Gaussian, the fitting is performed only from -10 to 2. Fig. 4.1 shows the fit in two momentum bins as an example. From the fit parameters, ratio of electrons which would pass the TPC cut to all electrons is determined. Fig. 4.2 shows the resulting efficiency.

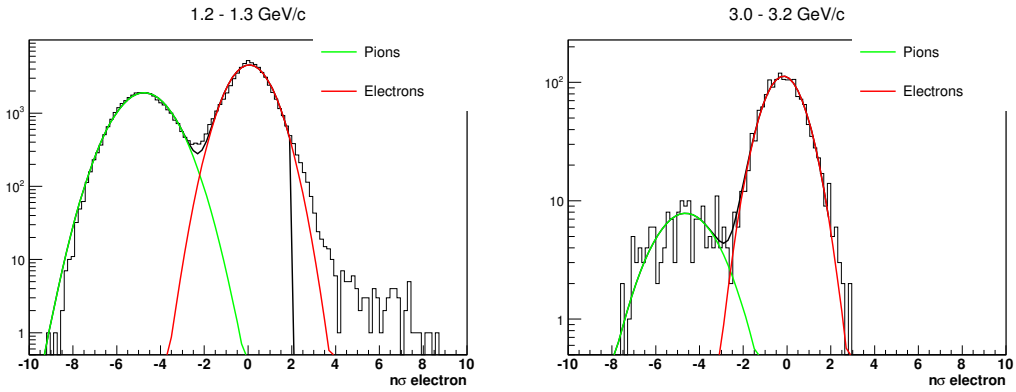

Figure 4.1: $n\sigma_e$ distribution for a pure electron sample for two momentum bins. Hadron contamination is still visible. The histogram is fitted with 2 Gaussians to describe electron and pion distribution.

4.1.2 TOF

TOF cut efficiency

Electrons are required to have $0,97 < 1/\beta < 1.025$. Cut efficiency for TOF is obtained by selecting a sample of photonic electrons using TPC and BEMC only. Then number of electrons fulfilling the TOF cut is determined. Since the electron distribution is Gaussian only approximately, the efficiency has been calculated as the ratio of electrons fulfilling the cut to those with $0,93 < 1/\beta < 1.07$. This second cut is chosen so it removes residual hadron contamination. The cut efficiency is shown in Fig. 4.3.

TOF matching efficiency

TOF acceptance is obtained from pure electron sample selected by TPC and BEMC only. Then the ratio of electrons from this sample, which have a valid TOF signal, to all electrons is studied. Fig. 4.4 shows the centrality dependence, Fig. 4.5 describes pseudorapidity dependence. To make the figure more organized, errors for pseudorapidity -1.0 – -0.8 are shown only. For the final calculation, pseudorapidity dependence was not considered and the efficiency was averaged over all pseudorapidities.

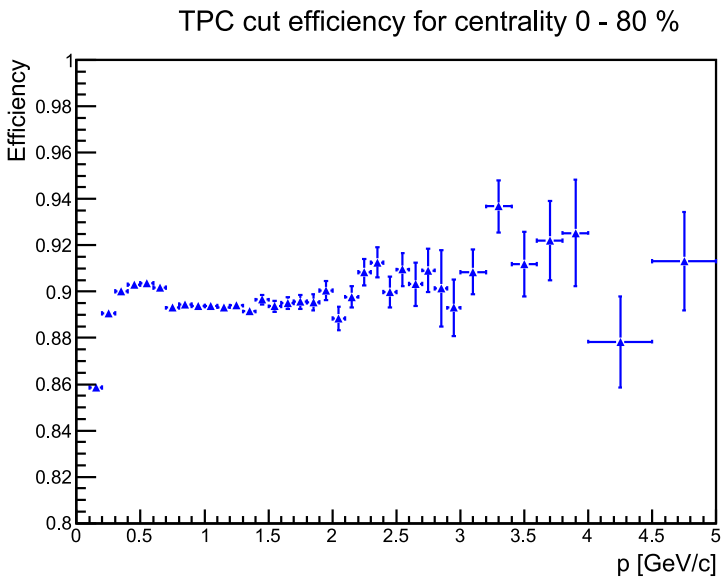

Figure 4.2: TPC cut efficiency as a function of electron momentum.

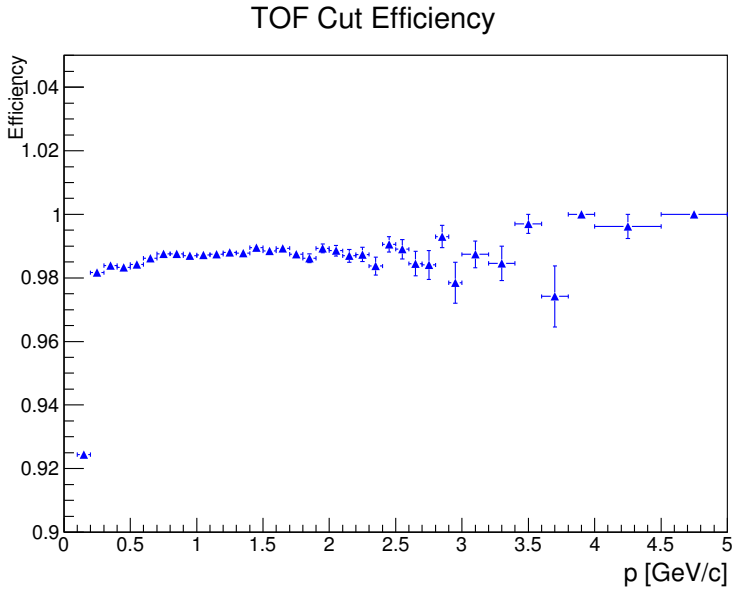

Figure 4.3: Efficiency of TOF cut as a function of momentum.

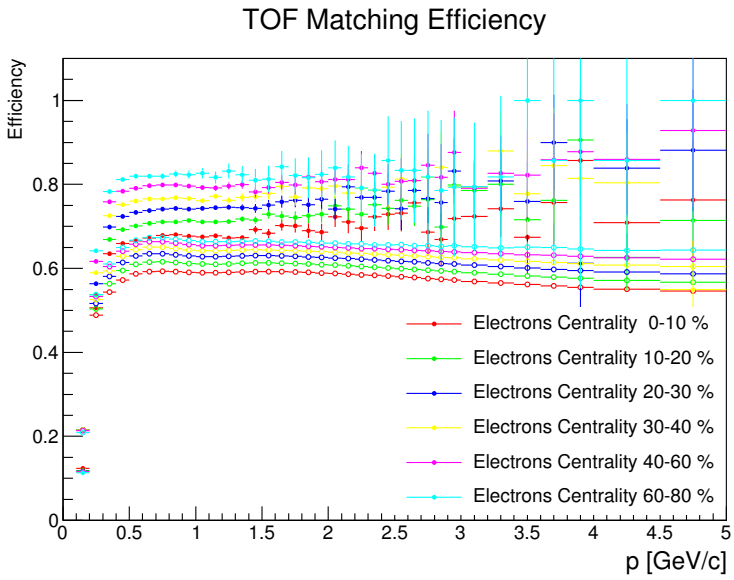

Figure 4.4: TOF matching efficiency for various centralities as a function of momentum.

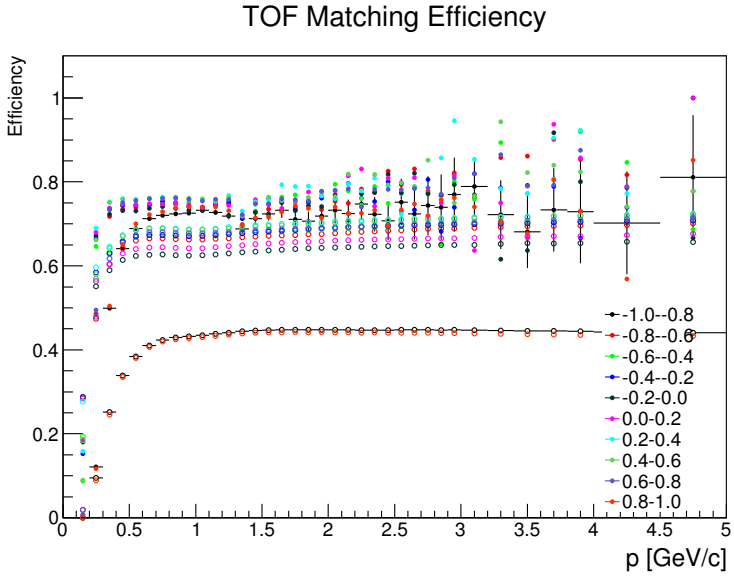

Figure 4.5: TOF matching efficiency for various pseudorapidities as a function of momentum. To improve clarity, errors are shown only for pseudorapidity -1.0 – -0.8. The errors are of similar magnitude for the remaining data points.

4.1.3 BEMC

BEMC cut efficiency

BEMC cut efficiency was extracted both from data and simulation. When using data, clear sample of photonic electrons is selected using TPC and TOF. In order to purify electron sample, the same–sign photonic pairs are subtracted. For the simulation, GEANT is used. As can be seen in Fig. 4.6, the agreement between the simulation and the data is very good. The efficiency is calculated as the ratio of electrons which fulfill the cut ($0.5 < E/p < 2.0$) to all of them. The results can be seen in Fig. 4.7, the difference between efficiency from data and simulation is about $(2 - 3)\,\%$

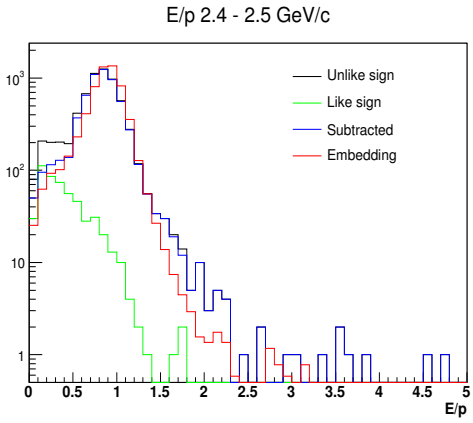

Figure 4.6: Distribution of E/p ratio for particles with momentum (2.4 – 2.5) GeV/c. Subtracted distribution is used for calculating the efficiency from data.

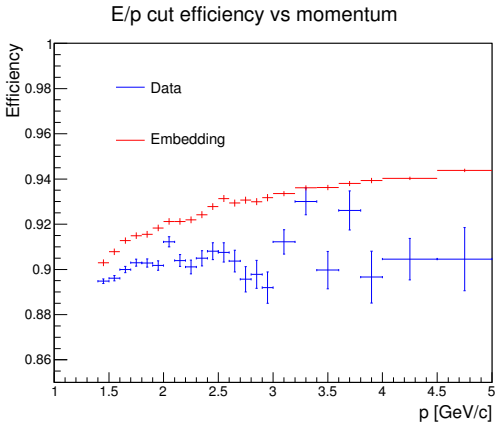

Figure 4.7: BEMC cut efficiency for two methods of extraction – from data and simulation. The average is used in the calculations of overall reconstruction efficiency.

BEMC matching efficiency

BEMC matching efficiency is determined from sample of photonic electrons selected by TPC only. TOF is not used because a probability that an electron will have a signal in the BEMC is not independent to a probability it will have a signal in TOF. In this manner we handle this dependence, which is then included in TOF matching efficiency. The resulting efficiency in the calorimeter can be seen in Fig. 4.8 and 4.9.

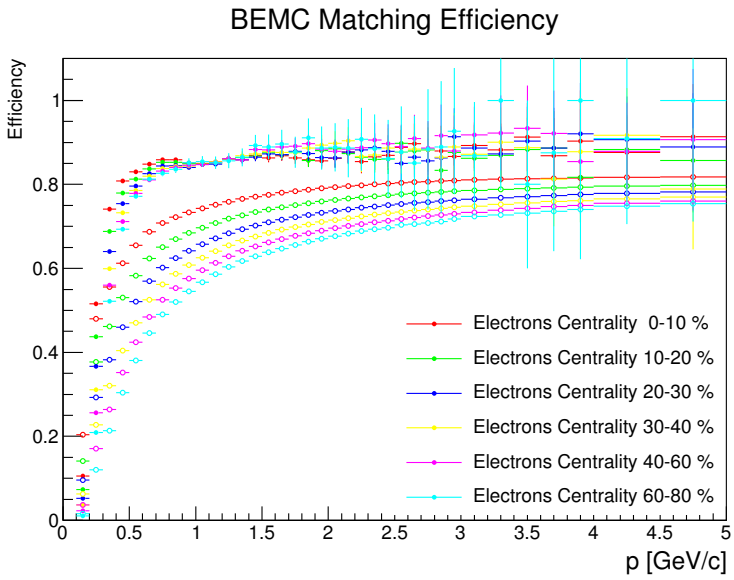

Figure 4.8: BEMC matching efficiency for various centralities as a function of momentum.

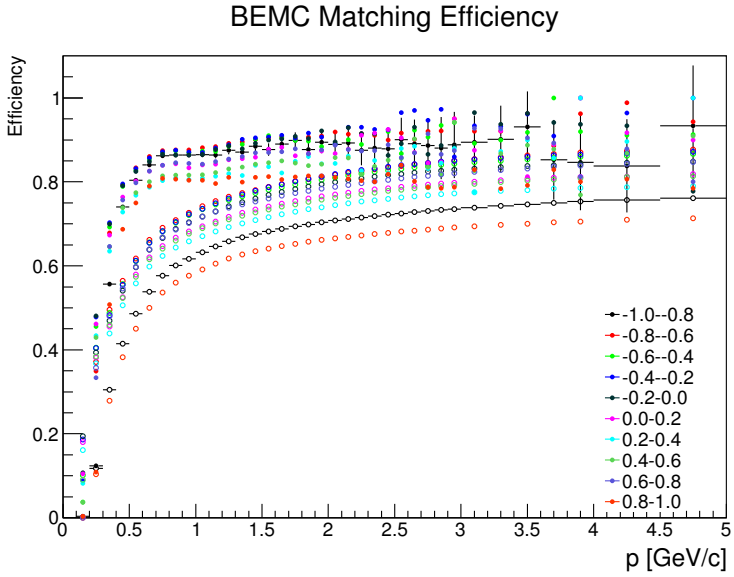

Figure 4.9: BEMC acceptance for various pseudorapidities as a function of momentum. Errors are shown only for pseudorapidity -1.0 – -0.8 in order to improve clarity. The errors are of similar magnitude for the remaining data points.

4.2 J/ψ reconstruction efficiency

Single electron PID efficiency (4.1) is calculated from detector efficiencies by bin multiplication. Resulting efficiency as a function of electron momentum is in Fig. 4.10. The discontinuity at $p = 1.4$ GeV/c is caused by the change in the cuts in TOF and due to the inclusion of BEMC for electron identification.

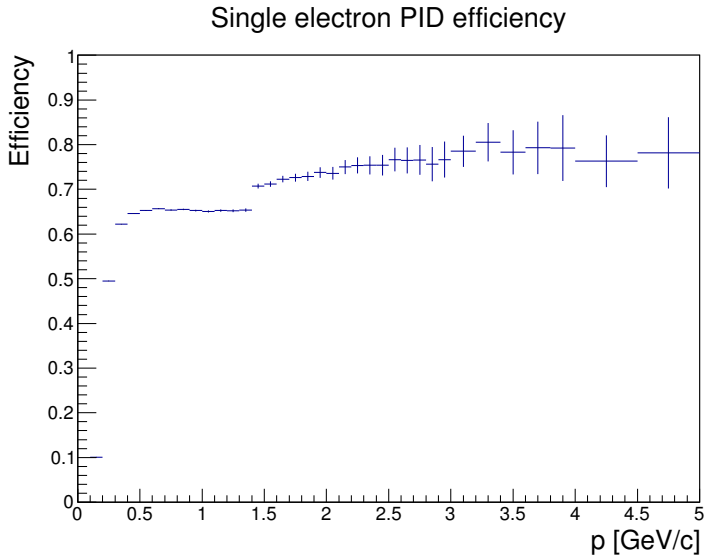

Figure 4.10: Single electron PID efficiency. This includes electron reconstruction efficiency in TOF and BEMC and also TPC cut efficiency.

4.2.1 TPC acceptance

TPC acceptance is obtained from embedding, where several J/ψ are generated in each collision and then their evolution in the detector is simulated by GEANT. These simulated hits are then added to real events and the particles are reconstructed using the same cuts on the track quality as in the analysis. Thus the number of simulated and also of reconstructed J/ψ is known. TPC acceptance is then obtained as a ratio of reconstructed to simulated J/ψ. Fig. 4.11 describes the geometrical and tracking efficiency as a function of transverse momentum.

4.2.2 Folding of the efficiencies

We have to fold the single electron efficiency and TPC acceptance together in order to obtain an overall detector efficiency. Since we want to correct

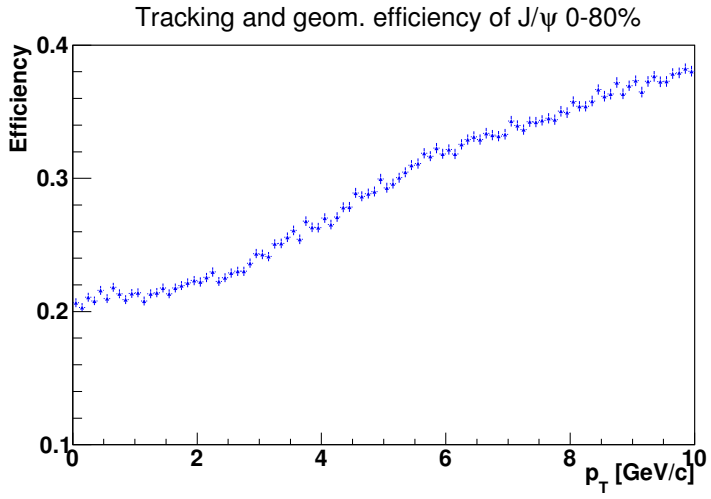

Figure 4.11: TPC geometrical and tracking efficiency for J/ψ.

our signal (section 3.6.1), it is desirable to determine the efficiency as a function of transverse momentum in a binning corresponding to the binning of our signal. First of all, we weighted our simulated J/ψ sample by the real transverse momentum distribution of J/ψ.

$$\frac{\mathrm{d}N}{\mathrm{d}p_{\mathrm{T}}} = \frac{A\,p_{\mathrm{T}}}{\left(1+(p_{\mathrm{T}}/b)^2\right)} \tag{4.2}$$

was used as the weighting function (obtained from [52]). The parameters A and b were determined iteratively by fitting the function (4.2) to the corrected spectra. The weighting ensures that J/ψ with higher momenta are not overrepresented – their number is proportional to the falling J/ψ spectrum. Next, momentum distribution of electron positron pairs for given bin of transverse momentum was generated by simulation. Fig. 4.12 shows an example of this distribution for J/ψ in bin with p_{T} (2.5 – 3.0) GeV/c. This distribution is then used to fold the single electron PID efficiencies (dependent on momentum) together and obtain efficiency for J/ψ, this time p_{T} dependent:

$$\epsilon_{\mathrm{folded}}(p_{\mathrm{T}}) = \epsilon_{\mathrm{TPCacc}}(p_{\mathrm{T}}) \times \sum_{p_{\mathrm{e}+},\,p_{\mathrm{e}-}} \epsilon_{\mathrm{sPID}}(p_{\mathrm{e}-}) \times \epsilon_{\mathrm{sPID}}(p_{\mathrm{e}+}) \times w \tag{4.3}$$

$\epsilon_{\mathrm{TPCacc}}(p_{\mathrm{T}})$ is the TPC geometrical and tracking efficiency in the given p_{T} bin. The sum in equation goes over all bins in momentum distribution of decay pairs. w is weight given to each bin and is defined as

$$w = \frac{N_{\mathrm{bin}}}{N_{\mathrm{all}}},$$

where N_{bin} is the number of decay pairs in the bin and N_{all} is the overall number of decay pairs. This procedure is repeated for every bin of J/ψ transverse momentum, resulting efficiency is shown in Fig. 4.13.

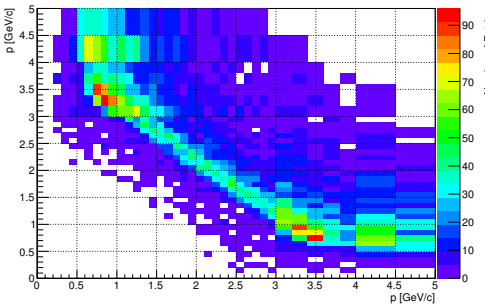

Figure 4.12: Distribution of momentum of electron positron pairs from J/ψ decays for J/ψ with transverse momentum (2.5 – 3.0) GeV/c.

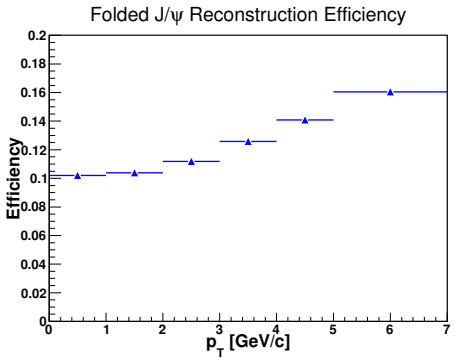

Figure 4.13: Folded J/ψ reconstruction efficiency as a function of p_{T}. The efficiency includes TPC, TOF and BEMC matching and cut efficiencies.

4.2.3 Signal counting correction

We determined the signal in 3.6 by bin counting in the invariant mass range from (2.9 – 3.2) GeV/c^2. Due to detector effects, not all of the J/ψ are reconstructed in this mass region. To estimate the ratio of the included J/ψ, embedding was used. It was then compared with our data to check if there is a good agreement. Fig. 4.14 presents this comparison. We got $\chi^2/\text{NDF} = 1.35$ in the mass region (2.6 – 3.6) GeV/c^2. The actual correction was then calculated as a ratio of J/ψ reconstructed in mass range (2.9 – 3.2) GeV/c^2 to all reconstructed J/ψ. This ratio was found to be 81.5 %.

There is an additional correction for signal counting: In the embedding, only J/$\psi \to \text{e}^+\,\text{e}^-$ decays are considered. However, we can not experimentally distinguish between these and J/$\psi \to \text{e}^+\,\text{e}^-\,\gamma$ decays. This adds another 9% correction in the considered mass window [53].

4.2.4 Overall reconstruction efficiency

Total J/ψ reconstruction efficiency is obtained from the folded efficiency 4.13 by applying signal counting corrections. Fig. 4.15 shows the result. The

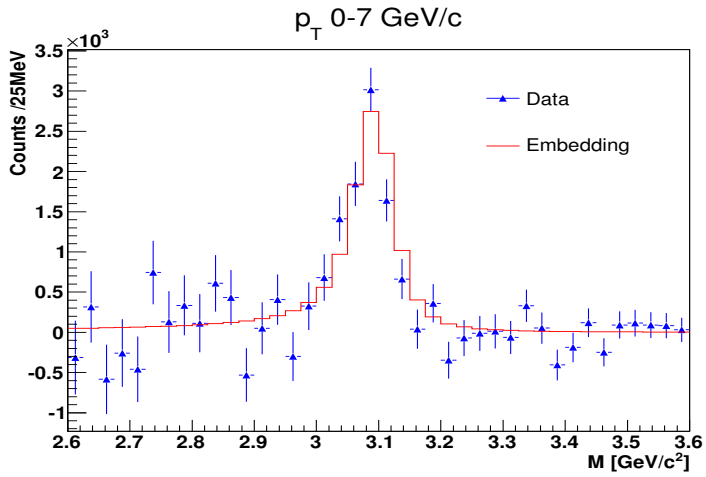

Figure 4.14: TPC geometrical and tracking efficiency for J/ψ.

overall reconstruction efficiency increases with p_{T} from 8 % to 13 % at 6 GeV/c.

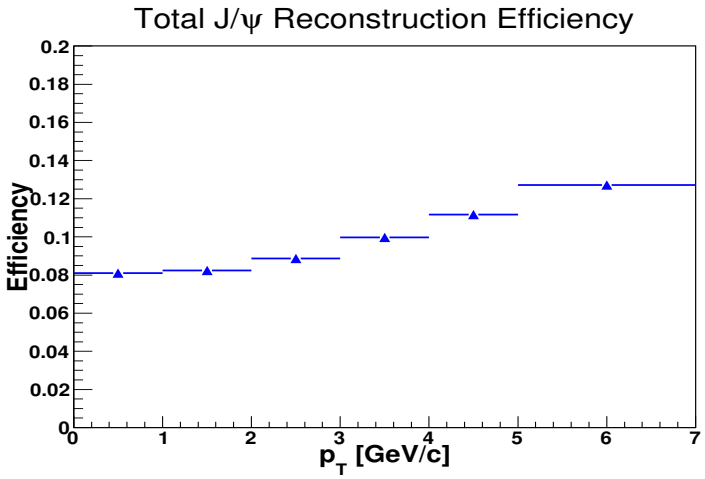

Figure 4.15: Overall J/ψ reconstruction efficiency. Statistical errors are included, but are smaller than triangles. Systematic uncertainty of the reconstruction is discussed in section 4.3.

4.3 Systematic uncertainty

4.3.1 Signal extraction

The systematic uncertainty of signal extraction was determined by varying several parameters. First, the invariant mass range, where the signal is counted, was extended from (2.9 – 3.2) GeV/c^2 to (2.7 – 3.2) GeV/c^2. Then the signal counting correction (discussed in detail in 4.2.3) for the new mass range was applied. The difference in yields, which was about 3 % was then taken as systematic uncertainty. The additional uncertainty originating in correction for $J/\psi \rightarrow e^+ e^- \gamma$ decays was estimated to be half of the correction, that is 5 %. This seems appropriate as the correction is based on theoretical calulation.

Another systematic uncertainty affecting signal comes from residual background. We do not have any simulation of the background. Its value was determined by fitting linear, second order polynomial and exponential function in two invariant mass ranges ((2.6 – 3.6) GeV/c^2 and (2.4 – 3.8) GeV/c^2, as described in 3.6) and then taking their average as the value of the residual background. The highest and lowest fit results differed by 10 % from the average value and this was taken as systematic uncertainty. Table 4.1 summarizes the systematic uncertainty orginating from the method of signal extraction. The overall value was calculated by adding individual terms quadratically.

	Systematic uncertainty (%)
Invariant mass range	±3
Radiative decays	±5
Residual background	±10
Signal extraction – overall	±12

Table 4.1: Summary of systematic uncertainty originating in signal extraction.

4.3.2 Particle identification

The systematic uncertainties in TPC, TOF and BEMC in U+U collisions are expected to be very similar to those in Au+Au collisions. Therefore, as

the first approximation, systematic errors were taken from [32] and are listed in table 4.2.

	Systematic uncertainty (%)
TPC cut	±6
TPC tracking	±7
TOF	±3
BEMC	±14
Overall	±17

Table 4.2: Summary of systematic uncertainty from detectors used for electron identification. The errors were taken from [32]

We also studied a difference between embedding and data for E/p ratio in BEMC. The difference in cut efficiency for single electron when calculated from data or from embedding can be seen in Fig. 4.7. Fig. 4.16 shows the difference in overall J/ψ reconstruction efficiency. Since the efficiency used for correcting signal was calculated from average value of BEMC cut efficiency, it is reasonable to take half of the difference as systematic uncertainty. Thus the systematic uncertainty ranges from 4.4 to 6.6 % depending on p_{T}. However, we already take this uncertainty into account in the BEMC systematic uncertainty of 14 % and so it is not included in the final calculation. Nevertheless, it serves as a crosscheck and will be useful when the uncertainties from table 4.2 are recalculated using U+U collisions.

4.3.3 Total systematic uncertainty

The overall systematic uncertainty is calculated from values in tables 4.1 and 4.2 as a square root of sum of squares of individual terms. It is found to be ± 20 %. However, this value is still subject for further studies.

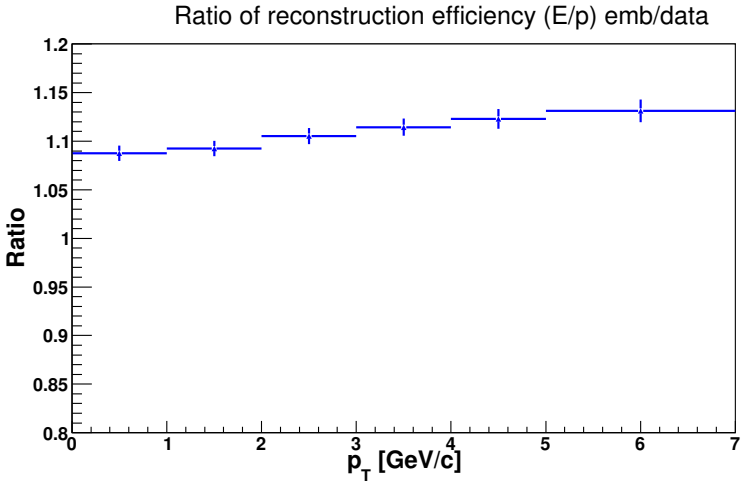

Figure 4.16: Ratio of overall J/ψ reconstruction efficiency calculated from embedding and from data.

Chapter 5

Results

The main results of the analysis are presented in this chapter: dependence of J/ψ invariant yield and nuclear modification factor on p_{T}.

5.1 Invariant yield

Invariant yield was calculated as

$$\frac{B}{2\pi p_{\mathrm{T}}}\frac{\mathrm{d}^2N}{\mathrm{d}y\,\mathrm{d}p_{\mathrm{T}}} = \frac{1}{2\pi p_{\mathrm{T}}\,\Delta p_{\mathrm{T}}\,\Delta y}\frac{N_{\mathrm{J}/\psi}}{N_{\mathrm{Ev}}}, \tag{5.1}$$

where B is the branching ratio (5.9 %), Δ denotes transverse momentum and rapidity bin width. $N_{\mathrm{J}/\psi}$ is number of J/ψ in a given bin after it was corrected with overall J/ψ reconstruction efficiency (see 4.2.4). N_{Ev} is number of events which were used in this analysis. There were 377 million events with minimum bias triggers, however only 0-80 % most central events were used, then some events were removed by events quality cuts (section 3.2), thus $N_{\mathrm{Ev}} = 296.7$ million events. Invariant yield was calculated as a function of transverse momentum (Fig. 5.1).

5.2 Nuclear modification factor

Nuclear modification factor (defined by (1.1)) has been computed as a function of transverse momentum, the equation (5.2) is rewritten R_{AA} using p+p cross section instead of yield.

$$R_{\mathrm{AA}}(p_{\mathrm{T}}, y) = \frac{\sigma_{\mathrm{inel}}\mathrm{d}^2N^{\mathrm{AA}}/\,\mathrm{d}p_{\mathrm{T}}\,\mathrm{d}y}{N_{\mathrm{coll}}\,\mathrm{d}^2\sigma^{\mathrm{pp}}/\,\mathrm{d}p_{\mathrm{T}}\,\mathrm{d}y}, \tag{5.2}$$

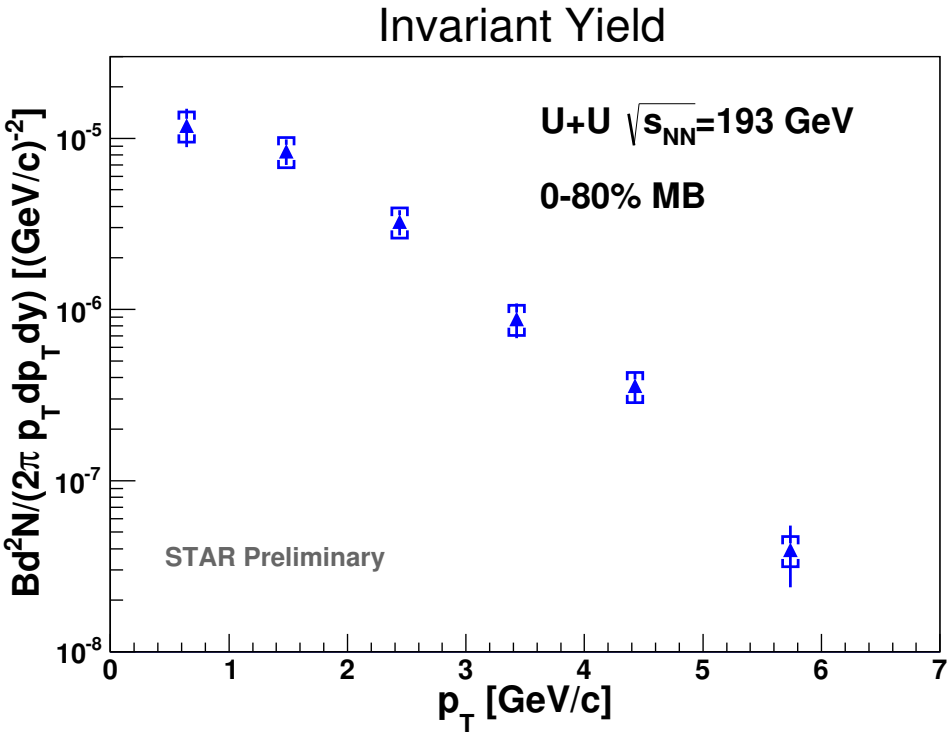

Figure 5.1: J/ψ invariant yield for 0-80 % most central U+U collisions. Vertical lines represent statistical uncertainty, brackets systematic uncertainty. Points are positioned in the mean value of their bins.

σ_{inel} is inelastic proton proton cross section, 42 ± 3 mb was used [54],[55]. Number of binary collisions N_{coll} was taken as 350 ± 36 based on [56]. In order to extract nuclear modification factor, baseline of p+p collisions is needed. There haven't been any p+p collisions at $\sqrt{s} = 193$ GeV, therefore collisions at $\sqrt{s} = 200$ GeV are used. We estimate that the difference is $\approx$ 3 % and will be included in the future. The other complication originates in the fact that current STAR measurement of J/ψ in p+p [25] has data points only for $p_{\text{T}} > 2$ GeV/c. To obtain low p_{T} points, the data from PHENIX were used [52]. PHENIX data have different rapidity, $|y| < 0.35$, we assumed that the production is the same as in rapidity $|y| < 1.0$. This method to obtain low p_{T} points is the same as used in Au+Au collisions at $\sqrt{s_{NN}} =$ 200 GeV, hence our results are directly comparable to STAR Au+Au results, as shown in Fig. 5.2.

We can see that the nuclear modification factor in U+U collisions at $\sqrt{s_{NN}} = 193$ GeV is similar to the one in Au+Au collisions at $\sqrt{s_{NN}} = 200$ GeV. There might be a hint of increase for higher p_{T}, however it is impossible

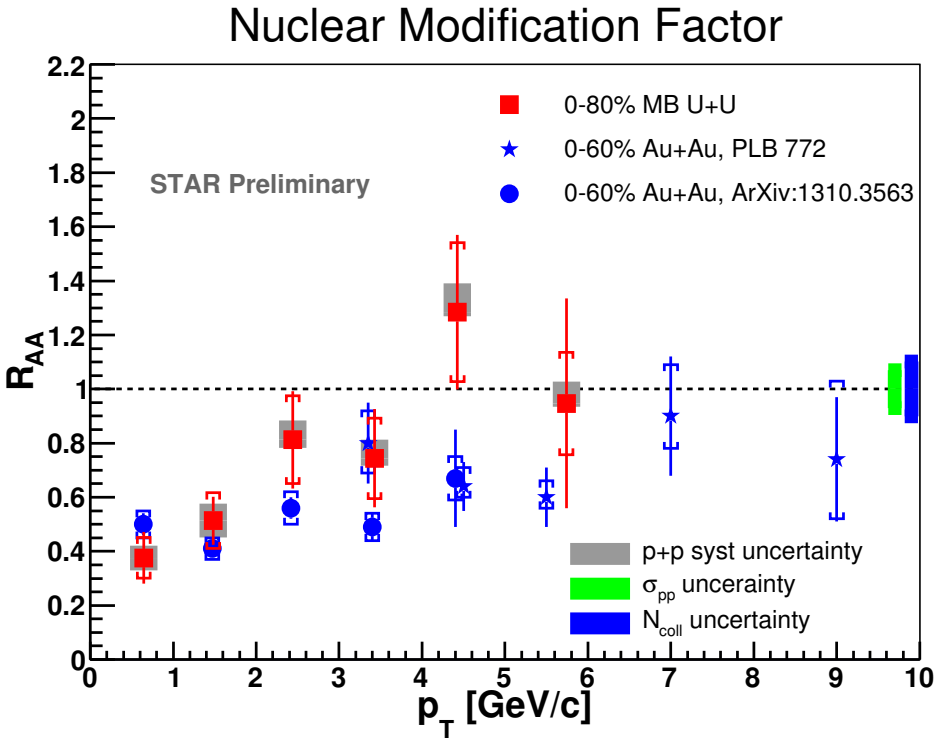

Figure 5.2: J/ψ nuclear modification factor as a function of p_{T}.. Vertical lines represent statistical uncertainty, brackets systematic uncertainty, grey, green and blue bands systematic uncertainty from p+p baseline, σ_{inel} and N_{coll} respectively. Au+Au points were taken from [32],[25].

to draw any strong conclusion if we consider the size of error bars. Please note that in U+U, 0-80 % most central collisions are used, while in Au+Au 0-60 % is shown. Since we expect stronger suppression (lower R_{AA}) for the more central collisions (for details see chapter 1), lower U+U R_{AA} than in the plot would be expected for the same centrality range. Centrality study of nuclear modification factor is currently being done.

This results on J/ψ R_{AA} and invariant yield are the main outcome of this analysis. They have been approved as STAR preliminary results and were presented at several conferences [57, 58, 59, 60] (see Appendix for more details), most notably at Quark Matter 2014 in Darmstadt.

Conclusions and outlook

In this diploma thesis, analysis of J/ψ in U+U collisions at $\sqrt{s_{NN}} = 193$ GeV at the STAR experiment was presented. Information from STAR subsystems – TPC, TOF and BEMC was used to obtain a raw signal with significance of 11 via dielectron decay channel J/$\psi \to e^+e^-$. The signal was then corrected for reconstruction efficiency using information from data or from Monte Carlo simulation. Study of systematic uncertainties was also performed.

The main result of the analysis is the extraction of J/ψ invariant yield and nuclear modification factor as a function of transverse momentum. We found that the J/ψ in U+U collisions is suppressed relatively to its production in p+p collisions in a similar manner as in Au+Au collisions at $\sqrt{s_{NN}} = 200$ GeV.

Next step in the analysis, which has already been started, is determination of R_{AA} centrality behavior. For that, centrally triggered data will be utilized as well. Then, data will be compared with relevant models and will improve our understanding of quarkonia in-medium dissociation. After the analysis is finalized, we expect that the work will be published as STAR result.

The preliminary results of the analysis have already been presented at several conferences, most notably at Quark Matter 2014. See Appendix for the overview of the presentations.

Bibliography

[1] J. C. Collins and M. J. Perry, "Superdense matter: Neutrons or asymptotically free quarks?," *Phys. Rev. Lett.*, vol. 34, pp. 1353–1356, May 1975.

[2] J. I. Kapusta, "Quantum Chromodynamics at High Temperature," *Nucl.Phys.*, vol. B148, pp. 461–498, 1979.

[3] E. V. Shuryak, "Quantum Chromodynamics and the Theory of Superdense Matter," *Phys.Rept.*, vol. 61, pp. 71–158, 1980.

[4] F. Karsch, "The Phase transition to the quark gluon plasma: Recent results from lattice calculations," *Nucl.Phys.*, vol. A590, pp. 367C–382C, 1995.

[5] R. Stock, "Relativistic Nucleus-Nucleus Collisions and the QCD Matter Phase Diagram," 2008. arXiv: 0807.1610.

[6] E. Eichten, K. Gottfried, T. Kinoshita, K. D. Lane, and T. M. Yan, "Charmonium: The model," *Phys. Rev. D*, vol. 17, pp. 3090–3117, Jun 1978.

[7] F. Karsch, M. Mehr, and H. Satz, "Color screening and deconfinement for bound states of heavy quarks," *Zeitschrift für Physik C Particles and Fields*, vol. 37, no. 4, pp. 617–622, 1988.

[8] K. Nakamura *et al.*, "Particle data group," *Journal of Physics G: Nuclear and Particle Physics*, vol. 37, no. 7A, p. 075021, 2010 and 2011 partial update for 2012 season.

[9] P. P. Bhaduri, P. Hegde, H. Satz, and P. Tribedy, "An Introduction to the Spectral Analysis of the QGP," *Lect.Notes Phys.*, vol. 785, pp. 179–197, 2010.

[10] T. Matsui and H. Satz, "J/psi Suppression by Quark-Gluon Plasma Formation," *Phys. Lett.*, vol. B178, p. 416, 1986.

[11] H. Satz, "Color deconfinement and J/ψ suppression in high-energy nuclear collisions," 1997.

[12] F. Karsch, "Deconfinement and quarkonium suppression," *Eur.Phys.J.*, vol. C43, pp. 35–43, 2005.

[13] C.-Y. Wong, "Heavy quarkonia in quark-gluon plasma," *Phys.Rev.*, vol. C72, p. 034906, 2005.

[14] H. Satz, "Quarkonium Binding and Dissociation: The Spectral Analysis of the QGP," *Nucl.Phys.*, vol. A783, pp. 249–260, 2007.

[15] P. Faccioli, C. Lourenco, J. Seixas, and H. Woehri, "Study of ψ' and χ_c decays as feed-down sources of J/ψ hadro-production," *JHEP*, vol. 0810, p. 004, 2008.

[16] Z. Tang, "J/psi production at high pT at STAR," *Nucl.Phys.*, vol. A855, pp. 396–399, 2011.

[17] R. L. Thews, M. Schroedter, and J. Rafelski, "Enhanced j/ψ production in deconfined quark matter," *Phys. Rev. C*, vol. 63, p. 054905, Apr 2001.

[18] P. Braun-Munzinger and J. Stachel, "(Non)thermal aspects of charmonium production and a new look at J / psi suppression," *Phys.Lett.*, vol. B490, pp. 196–202, 2000.

[19] A. Andronic, P. Braun-Munzinger, K. Redlich, and J. Stachel, "The thermal model on the verge of the ultimate test: particle production in Pb-Pb collisions at the LHC," *J.Phys.*, vol. G38, p. 124081, 2011.

[20] "A new measurement of j/ψ suppression in pb-pb collisions at 158 gev per nucleon," *The European Physical Journal C - Particles and Fields*, vol. 39, no. 3, pp. 335–345, 2005.

[21] R. Vogt, "Shadowing and absorption effects on J/psi production in dA collisions," *Phys.Rev.*, vol. C71, p. 054902, 2005.

[22] J. Aubert *et al.*, "Measurements of the nucleon structure functions $F2_n$ in deep inelastic muon scattering from deuterium and comparison with those from hydrogen and iron," *Nucl.Phys.*, vol. B293, p. 740, 1987.

[23] M. Arneodo, "Nuclear effects in structure functions," *Phys.Rept.*, vol. 240, pp. 301–393, 1994.

[24] S. Gavin and M. Gyulassy, "Transverse-momentum dependence of j/ψ production in nuclear collisions," *Physics Letters B*, vol. 214, no. 2, pp. 241 – 246, 1988.

[25] L. Adamczyk *et al.*, "J/ψ production at high transverse momenta in $p+p$ and Au+Au collisions at $\sqrt{s_{NN}} = 200$ GeV," *Phys.Lett.*, vol. B722, pp. 55–62, 2013.

[26] Q. Hao and Star Collaboration, "Heavy Flavor Results from STAR," *Journal of Physics Conference Series*, vol. 422, p. 012013, Mar. 2013.

[27] B. Trzeciak, "Quarkonia production in the STAR experiment," *Nucl.Phys.A904-905*, vol. 2013, pp. 607c–610c, 2013.

[28] A. Adare *et al.*, "Transverse-Momentum Dependence of the J/ψ Nuclear Modification in d+Au Collisions at $\sqrt{s_{NN}} = 200$ GeV," *Phys.Rev.*, vol. C87, no. 3, p. 034904, 2013.

[29] K. J. Eskola, H. Paukkunen, and C. A. Salgado, "EPS09 - Nuclear PDFs and Their Uncertainties at NLO," *Nucl.Phys.*, vol. A830, pp. 599C–602C, 2009.

[30] X. Zhao and R. Rapp, "Charmonium in Medium: From Correlators to Experiment," *Phys.Rev.*, vol. C82, p. 064905, 2010.

[31] Y.-p. Liu, Z. Qu, N. Xu, and P.-f. Zhuang, "J/psi Transverse Momentum Distribution in High Energy Nuclear Collisions at RHIC," *Phys.Lett.*, vol. B678, pp. 72–76, 2009.

[32] L. Adamczyk *et al.*, "J/ψ production at low p_T in Au+Au and Cu+Cu collisions at $\sqrt{s_{NN}} = 200$ GeV at STAR," 2013.

[33] S. Chatrchyan *et al.*, "Suppression of non-prompt J/ψ, prompt J/ψ, and Y(1S) in PbPb collisions at $\sqrt{s_{NN}} = 2.76$ TeV," *JHEP*, vol. 1205, p. 063, 2012.

[34] D. Kikola, G. Odyniec, and R. Vogt, "Prospects for quarkonia production studies in U + U collisions," *Phys.Rev.*, vol. C84, p. 054907, 2011.

[35] G. Wang, "Search for chiral magnetic effects in high-energy nuclear collisions," *Nuclear Physics A*, vol. 904-905, no. 0, pp. 248c – 255c, 2013.

[36] R. Snellings, "Elliptic Flow: A Brief Review," *New J.Phys.*, vol. 13, p. 055008, 2011.

[37] M. L. Miller, K. Reygers, S. J. Sanders, and P. Steinberg, "Glauber modeling in high energy nuclear collisions," *Ann.Rev.Nucl.Part.Sci.*, vol. 57, pp. 205–243, 2007.

[38] M. Kliemant, R. Sahoo, T. Schuster, and R. Stock, "Global Properties of Nucleus-Nucleus Collisions," *Lect.Notes Phys.*, vol. 785, pp. 23–103, 2010.

[39] M. Anderson, J. Berkovitz, W. Betts, R. Bossingham, F. Bieser, *et al.*, "The Star time projection chamber: A Unique tool for studying high multiplicity events at RHIC," *Nucl.Instrum.Meth.*, vol. A499, pp. 659–678, 2003.

[40] STAR TOF Collaboration, "Proposal for a Large Area Time of Flight System for STAR," 2004.

[41] M. Beddo, E. Bielick, T. Fornek, *et al.*, "The STAR Barrel Electromagnetic Calorimeter," *Nucl.Instrum.Meth.*, vol. A499, pp. 725–739, 2003.

[42] C. Adler, A. Denisov, E. Garcia, M. J. Murray, H. Strobele, *et al.*, "The RHIC zero degree calorimeter," *Nucl.Instrum.Meth.*, vol. A470, pp. 488–499, 2001.

[43] W. Llope, F. Geurts, J. Mitchell, Z. Liu, N. Adams, *et al.*, "The TOFp / pVPD time-of-flight system for STAR," *Nucl.Instrum.Meth.*, vol. A522, pp. 252–273, 2004.

[44] A. Adare *et al.*, "J/ψ Production vs Centrality, Transverse Momentum, and Rapidity in Au+Au Collisions at $\sqrt{s_{NN}} = 200$ GeV," *Phys.Rev.Lett.*, vol. 98, p. 232301, 2007.

[45] L. Ruan, "Personal Correspondence." 2014.

[46] L. Ruan, G. Lin, Z. Xu, K. Asselta, H. Chen, *et al.*, "Perspectives of a Midrapidity Dimuon Program at RHIC: A Novel and Compact Muon Telescope Detector," *J.Phys.*, vol. G36, p. 095001, 2009. Updated at http://www.star.bnl.gov/ ruanlj/MTDreview2010/MTD_proposal_v14.pdf.

[47] D. Beavis *et al.*, "The STAR Heavy flavor Tracker Conceptual Design Report." November 2009.

[48] D. Beavis *et al.*, "The STAR Heavy flavor Tracker Technical Design Report." June 2011.

[49] O. Kukral, "Production of J/ψ in U+U collisions at the STAR Experiment." Research project, 2013.

[50] H. Matsui, "Preliminary centrality definitions in U+U." Internal STAR presentation, May 2013.

[51] T. Skwarnicki, "A study of the radiative CASCADE transitions between the Upsilon-Prime and Upsilon resonances," 1986.

[52] A. Adare *et al.*, "Transverse momentum dependence of J/psi polarization at midrapidity in p+p collisions at $\sqrt{s_{NN}}$ = 200 GeV," *Phys.Rev.*, vol. D82, p. 012001, 2010.

[53] A. Spiridonov, "Bremsstrahlung in leptonic onia decays: Effects on mass spectra," 2004.

[54] B. Abelev *et al.*, "Systematic Measurements of Identified Particle Spectra in pp, d^+ Au and Au+Au Collisions from STAR," *Phys.Rev.*, vol. C79, p. 034909, 2009.

[55] J. Adams *et al.*, "phi meson production in Au + Au and p+p collisions at $\sqrt{s_{NN}}$ = 200 GeV," *Phys.Lett.*, vol. B612, pp. 181–189, 2005.

[56] H. Masui, B. Mohanty, and N. Xu, "Predictions of elliptic flow and nuclear modification factor from 200 GeV U + U collisions at RHIC," *Phys.Lett.*, vol. B679, pp. 440–444, 2009.

[57] W. Zha, "Quarkonium production in p+p and A+A from STAR." Presentation Quark Matter 2014, May 2014.

[58] O. Kukral, "J/ψ production in minimum bias U+U collisions at 193 GeV in the STAR experiment." Poster at Quark Matter 2014, May 2014.

[59] O. Kukral, "J/ψ production in A+A collisions at STAR." Presentation at 2014 RHIC & AGS Annual Users' Meeting, June 2014.

[60] R. Vertesi, "Heavy Flavor Measurements at STAR." Presentation at ICHEP 2014, July 2014.

Appendix

Presentations

Preliminary results and parts of the analysis have been presented in person at several conferences, most notably at:

- 2013 European Physical Society Conference on High Energy Physics (**EPS-HEP 2013**) at Stockholm, Sweden, as a poster presentation. Proceedings from the conference have been published at Proceedings of Science.
- Indian Summer School 2013 at Prague, Czech republic, as an oral presentation.
- The 6th International Conference on Hard and Electromagnetic Probes of High-Energy Nuclear Collisions (**Hard Probes 2013**) at Cape Town, South Africa, as a poster presentation.
- Zimányi Winter School 2013 at Budapest, Hungary, as a part of an oral presentation about J/ψ measurements at STAR.
- XXIV International Conference on Ultrarelativistic Nucleus–Nucleus Collisions (**Quark Matter 2014**) at Darmstadt, Germany, as a poster presentation.
- 2014 RHIC & AGS Annual Users' Meeting at BNL, USA, as a part of an oral presentation about J/ψ measurements at STAR.

In the following pages, poster and proceedings from EPS-HEP 2013 and poster from Quark Matter 2014 are shown.

J/ψ production in U+U collisions at 193 GeV in the STAR experiment

Ota Kukral* for the STAR Collaboration

Faculty of Nuclear Sciences and Physical Engineering
Czech Technical University, Prague

Abstract

Extensive studies of properties of quark-gluon plasma (QGP), the partonic matter created in heavy ion collisions, have been conducted at RHIC for over a decade. Suppression of quarkonia production in high energy nuclear collisions relative to proton-proton collisions, due to Debye screening of the quark-antiquark potential, has been predicted to be a sensitive indicator of the temperature of the created QGP. However, initial-state nuclear effects on the parton distributions (shadowing), production via recombination of quark-antiquark pairs in the QGP and dissociation in hadronic phase could also alter the expected suppression picture. Systematic measurements of the quarkonia production for different colliding systems are required to understand the quarkonium interactions with the partonic medium, and then the QGP properties. To further study the pattern of quarkonia suppression we can utilize the collisions of non-spherical nuclei such as uranium.
In this poster, we present the analysis status on J/ψ production, reconstructed at midrapidity via di-electron decay channel, in U+U collisions at $\sqrt{s_{NN}}$ = 193 GeV in the STAR experiment.

Motivation

Measurements of J/ψ in-medium dissociation in heavy ion collisions are expected to provide an estimate of the initial temperature of the system. The interpretation of medium induced modification requires a good understanding of its production mechanisms in p+p collisions and cold nuclear matter effects in d+Au collisions.
In STAR, J/ψ was measured in p+p, d+Au, Au+Au [1] and Cu+Cu collisions at $\sqrt{s_{NN}}$ = 200 GeV and Au+Au collisions at $\sqrt{s_{NN}}$ = 39 GeV and 62 GeV.

- **Top picture** [2]: R_{AA} dependence on centrality of a collision for all p_T and for high p_T only. J/ψ suppression in Au+Au increases with a centrality and decreases toward higher p_T across the centrality range. The data are compared to models that include contributions from prompt production and statistical charm quark regeneration [3,4]
- **Bottom picture** [5]: Charged tracks multiplicity for Au+Au and U+U collisions. Top values of charged tracks multiplicity are higher in U+U collisions, which is caused by higher initial energy density (due to prolate shape of uranium nucleus).

Higher achievable energy density in uranium collisions could be used to further study quarkonia production [6].

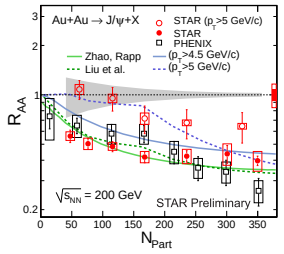

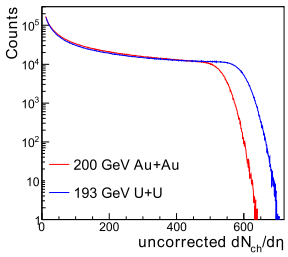

Data Analysis

Data used are 377M minimum bias uranium collisions at $\sqrt{s_{NN}}$ = 193 GeV taken in 2012.
Electrons are selected from good trajectories using TPC, TOF and BEMC:

TPC

- nσ - distance from the expected mean value of the energy loss expressed as number of standard deviations
- -1.5 < nσ electron < 2
- |nσ pion| > 2.5

TOF

- 0.97 < 1/β < 1.03
- Used: • p < 1.4 GeV/c — strictly required
  • p > 1.4 GeV/c — only if the particle has a TOF signal

BEMC

- Used only for p > 1.4 GeV/c
- 0.3 < p/E < 1.5

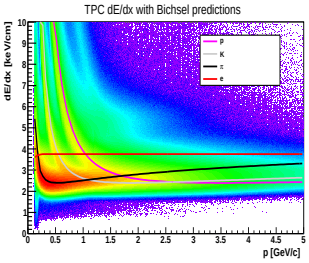

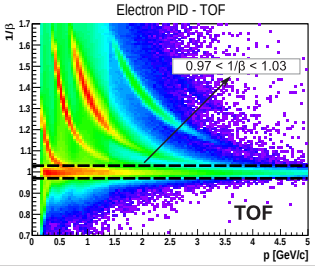

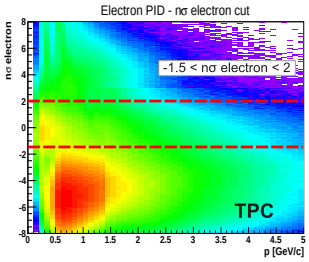

STAR Experiment

The Solenoidal Tracker At RHIC is a multi-purpose detector exceling at tracking and identification of charged particles at mid-rapidity in the high multiplicity environment of heavy ion collisions. The main subsystems used in this analysis are:

Time Projection Chamber (TPC)

- Full 2π azimuthal coverage
- Pseudorapidity -1.3 < η < 1.3
- Charged particle tracking and momentum reconstruction
- Particle identification via specific ionization energy loss dE/dx

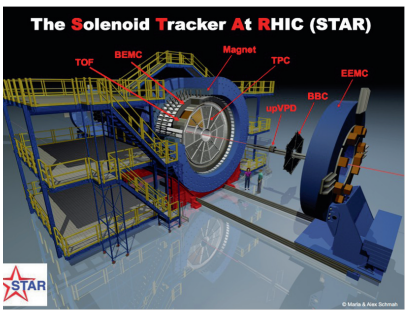

Time of Flight (TOF)

- Timing resolution <100 ps
- Particle identification via 1/β
- Together with TPC provides a good separation of electrons from heavier hadrons up to about 1.5 GeV/c

Barrel Electromagnetic Calorimeter (BEMC)

- Tower Δη×Δφ = 0.05×0.05
- Electron-hadron separation using p/E at high momentum

Results

- J/ψ → e^+e^- channel used for the analysis (branching ratio 5.9%)
- Combinatorial background reconstruction: Like-sign method ($e^+e^+ + e^-e^-$ pairs)
- Signal significance calculated in mass region (2.9 - 3.2) GeV/c^2 as $sg = \frac{S}{\sqrt{S+2B}}$
- S = 9440 ± 640 with significance 12.9 σ
- Signal divided into 11 p_T bins from 0 to 7 GeV/c with significance from 3.0 to 6.5 σ

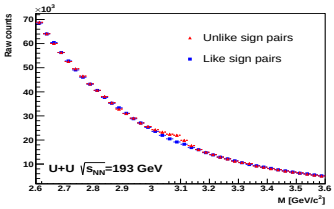

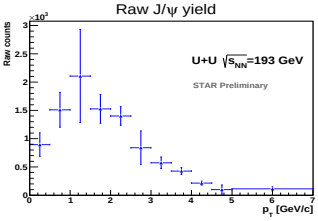

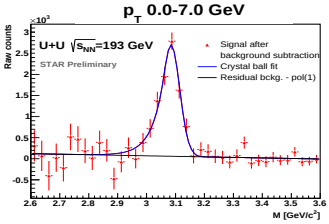

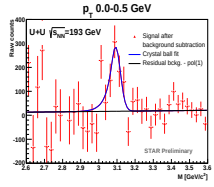

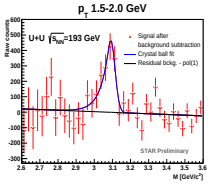

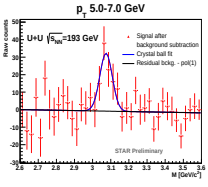

Conclusions and Perspectives

- J/ψ signal of significance of 12.9 σ observed
- Signal was divided into several p_T bins
- Studies of efficiency corrections and detectors effects are currently underway

References

[1] L. Adamczyk et al. [STAR Collaboration], Phys. Lett. B722, 55-62 (2013)
[2] H.Qiu (for the STAR Collaboration), J. Phys. Conf. Ser. 422, 012013 (2013)
[3] Y. Liu et al., Phys. Lett B678, 72 (2009)
[4] X. Zhao and R. Rapp, Phys. Rev. C82, 064905 (2010)
[5] G. Wang, Nuclear Physics A904–905, 248c-255c (2013)
[6] D. Kikola et al., Phys.Rev. C84,054907 (2011)

Acknowledgements

This work was supported by the grant of the Grant Agency of Czech Republic n. 13-20841S and by the Grant Agency of the Czech Technical University in Prague, grant No. SGS13/215OHK4/3T/14.

* kukral@rcf.rhic.bnl.gov.

Presented at the 2013 European Physical Society Conference on High Energy Physics, Stockholm, Sweden, 18-24 July, 2013

PROCEEDINGS OF SCIENCE

J/ψ production in U+U collisions at $\sqrt{s_{NN}} = 193$ GeV in the STAR experiment

Ota Kukral* **for the STAR Collaboration**
Department of Physics, Faculty of Nuclear Sciences and Physical Engineering, Czech Technical University in Prague, Czech Republic
E-mail: kukral@rcf.rhic.bnl.gov

Extensive studies of quark-gluon plasma (QGP), the novel state of strongly interacting matter governed by partonic degrees of freedom, have been conducted at RHIC for over a decade. Suppression of quarkonia production in high energy nuclear collisions relative to proton-proton collisions, due to Debye screening of the quark-antiquark potential, has been predicted to be a sensitive indicator of the temperature of the created QGP. However, cold nuclear matter effects, production via recombination of quark-antiquark pairs in the QGP and dissociation in hadronic phase could also alter the expected suppression picture. Indeed, recent measurements in Au+Au and d+Au collisions show that these effects play a non-negligible role. Hence systematic measurements of the quarkonia production for different colliding systems are crucial for understanding the quarkonium interactions with the partonic medium, and then the QGP properties. To further study the pattern of quarkonia suppression we can utilize the collisions of non-spherical nuclei such as uranium. In this paper, we will present the analysis status on J/ψ production, measured at midrapidity via di-electron decay channel, in U+U collisions at $\sqrt{s_{NN}} = 193$ GeV in the STAR experiment.

The European Physical Society Conference on High Energy Physics -EPS-HEP2013
18-24 July 2013
Stockholm, Sweden

*Speaker.

1. Motivation

Measurements of J/ψ in-medium dissociation in heavy ion collisions are expected to provide an estimate of the initial temperature of the system [1]. To understand medium induced modification it is beneficial to study J/ψ in various colliding systems. In STAR, J/ψ has been measured in p+p, d+Au, Au+Au and Cu+Cu collisions at $\sqrt{s_{NN}} = 200$ GeV [2][3] and Au+Au collisions at $\sqrt{s_{NN}} = 39$ GeV and 62 GeV [4]. U+U collisions are of interest since uranium nucleus is non-spherical, which leads to higher initial energy density not only in tip-to-tip collision, but even when averaged over all possible orientations of colliding nuclei [5][6].

2. Data Analysis

STAR is a multi-purpose detector excelling at tracking and identification of charged particles at mid-rapidity in the high multiplicity environment of heavy ion collisions. The main subsystems used for electron selection in this analysis are:

– Time Projection Chamber (TPC): momentum reconstruction together with particle identification via specific ionization energy loss $\mathrm{d}E/\mathrm{d}x$.
– Time of Flight (TOF): particle identification by measuring velocity β.
– Barrel Electromagnetic Calorimeter (BEMC): electron-hadron separation via momentum/energy ratio.

These results are based on analysis of 377 millions of minimum bias uranium collisions at $\sqrt{s_{NN}} = 193$ GeV taken in 2012 by the STAR experiment at RHIC. Sample of 0-80 % most central events with vertex z position within 30 cm of the center of the detector are used. Electrons were selected from good quality tracks by requiring $-1.5 < n\sigma_{\mathrm{electron}} < 2$ and $|n\sigma_{\mathrm{pion}}| > 2.5$ where $n\sigma$ is a distance from the expected mean value of the energy loss expressed as a number of standard deviations. The value of $1/\beta$ was required to be between 0.97 and 1.03. This cut has to be fulfilled for all particles with momentum lower then 1.4 GeV/c, for particles with p > 1.4 GeV/c the cut is applied only if they have a valid TOF signal. For particles with p > 1.4 GeV/c information from BEMC is also used for electron-hadron separation requiring the ratio 0.3 < p/E < 1.5, where E is an energy deposited by particle in a single BEMC tower. This takes advantage of the fact that electrons, unlike hadrons, deposit most of their energy in the calorimeter. Fig. 1 shows $n\sigma_{\mathrm{electron}}$ and $1/\beta$ distributions and applied cuts.

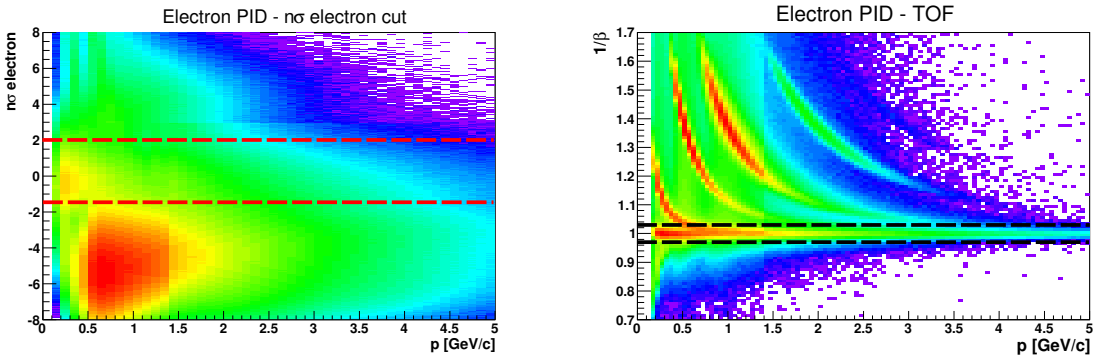

Figure 1: Left: TPC $n\sigma_{\mathrm{electron}}$ for particles which have already fulfiled TOF and BEMC cuts. Right: TOF $1/\beta$ vs. momentum for particles which have already passed TPC and BEMC cuts. Dashed lines show the selected region.

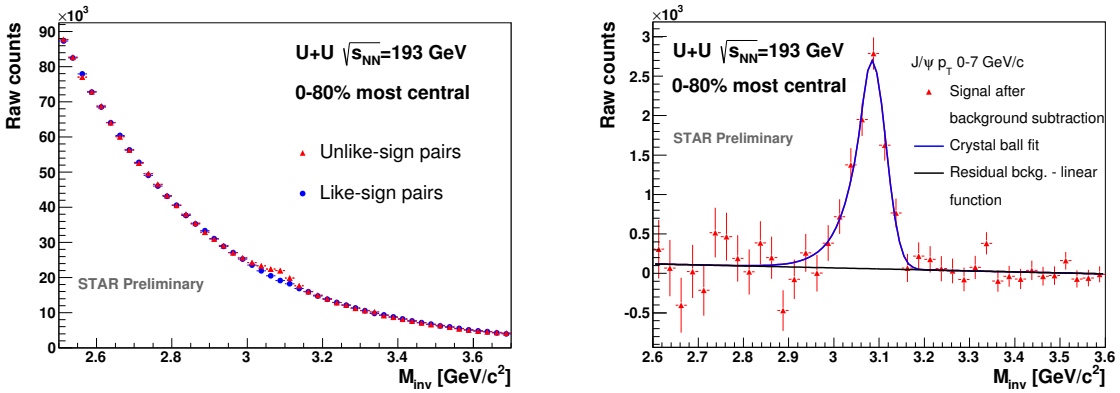

Figure 2: Left: Invariant mass of unlike-sign and like-sign electron (positron) pairs in 0-80 % most central U+U collisisons at $\sqrt{s_{NN}} = 193$ GeV. Right: Signal after background subtraction fitted with crystal ball function superimposed on a linear residual background.

3. Results and Summary

J/ψ is reconstructed via di-electron decay channel with branching ratio of 5.9 %. Combinatorial background is reconstructed using invariant mass of like-sign pairs. Signal after background subtraction is than fitted with crystal ball function to describe the signal and linear function to account for residual background. Signal before and after combinatorial background subtraction is shown on Fig. 2. Signal in mass region $(2.9-3.2)$ GeV/c^2 is 9440 ± 640 with significance of 12.9σ. This will make possible to divide the signal into several p_{T} bins going up to 7 GeV/c.

To conclude, in this work we have presented the current status of J/ψ analysis in U+U collisions at $\sqrt{s_{NN}} = 193$ GeV collected by the STAR experiment. Strong J/ψ signal has been observed in 0-80 % most central miminum bias collisions. This available statistics will allow us to extract nuclear modification factor $\mathrm{R_{AA}}$ as a function of p_{T} and centrality, therefore shedding more light on the effects associated with in-medium dissociation of heavy quarkonia.

Acknowledgments

This analysis was supported by the grant of the Grant Agency of Czech Republic n. 13-20841S and by the Grant Agency of the Czech Technical University in Prague, grant No. SGS13 /215OHK4/3T/14.

References

[1] T. Matsui and H. Satz, *J/psi Suppression by Quark-Gluon Plasma Formation*, Phys.Lett. **B178**, 416 (1986).

[2] L. Adamczyk et al. [STAR Collaboration], *J/ψ production at high transverse momenta in $p+p$ and Au+Au collisions at $\sqrt{s_{NN}} = 200$ GeV*, Phys.Lett. **B722**, 55-62 (2013).

[3] H. Qiu, *Heavy Flavor Results from STAR*, J.Phys.: Conf. Ser. **422** 012013 (2013).

[4] B. Trzeciak et al. [STAR Collaboration], *Quarkonia production in the STAR experiment*, Nucl.Phys. **A904-905**, 607c (2013).

[5] D. Kikola et al., *Prospects for quarkonia production studies in U+U collisions*, Phys. Rev. **C84** 054907 (2011).

[6] G. Wang, *Search for Chiral Magnetic Effects in High-Energy Nuclear Collisions*, Nucl.Phys. **A904-905**, 248c-255c (2013).

J/ψ production in minimum bias U+U collisions at 193 GeV in the STAR experiment

Ota Kukral* for the STAR Collaboration

Faculty of Nuclear Sciences and Physical Engineering
Czech Technical University, Prague

Abstract

Suppression of quarkonium production in high-energy nuclear collisions relative to proton-proton collisions, due to color screening of the quark-antiquark potential, has been predicted to be a sensitive indicator of the temperature of the created QGP. However, initial state cold nuclear matter effects, production via recombination of quark-antiquark pairs in the QGP and dissociation in hadronic phase could also alter the expected suppression picture. Systematic measurements of the quarkonium production in different colliding systems are hence crucial for disentangling relative contributions of these effects. At the STAR experiment we can utilize collisions of uranium nuclei to further study the quarkonia suppression pattern. Since the uranium nuclei are non-spherical and larger than Au nuclei, we are able to reach higher energy densities in the most central U+U collision compared to Au+Au collisions. In this poster, we will present the transverse momentum spectrum ($0 < p_T < 6$ GeV/c) and nuclear modification factor of J/ψ production, reconstructed at midrapidity via di-electron decay channel, in minimum bias U+U collisions at $\sqrt{s_{NN}}$ = 193 GeV in the STAR experiment.

Motivation

Measurements of J/ψ in-medium dissociation in heavy ion collisions are expected to provide an estimate of the initial temperature of the system. However, the interpretation of such medium-induced modification requires a good understanding of J/ψ production mechanisms in p+p collisions and cold nuclear matter effects in d+Au collisions.
Higher achievable energy density in uranium collisions could be used to further study quarkonium production [1].

- **Top picture** [2,3]: R_{AA} dependence on centrality of Au+Au collisions for all p_T and for high p_T only. J/ψ suppression in Au+Au increases with the centrality and decreases toward higher p_T across the measured centrality range. The data are compared to models that include contributions from prompt production and statistical charmonium regeneration [4,5]
- **Bottom picture** [6]: Charged-track multiplicity for Au+Au and U+U collisions. Top values of charged-track multiplicity are higher in U+U collisions, which is caused by higher initial energy density.

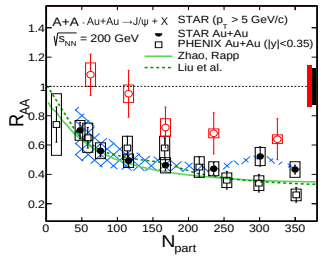

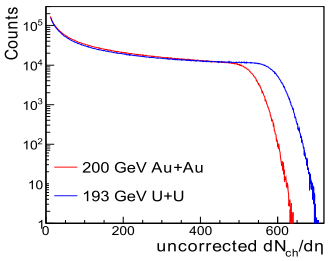

STAR Experiment

The Solenoidal Tracker At RHIC (STAR) is a multi-purpose detector exceling at tracking and identification of charged particles at mid-rapidity in the high multiplicity environment of heavy-ion collisions. The main subsystems used in this analysis are:

Time Projection Chamber (TPC)

- Full 2π azimuthal coverage
- Pseudorapidity -1.3 < η < 1.3
- Charged particle tracking and momentum reconstruction
- Particle identification via ionization energy loss dE/dx

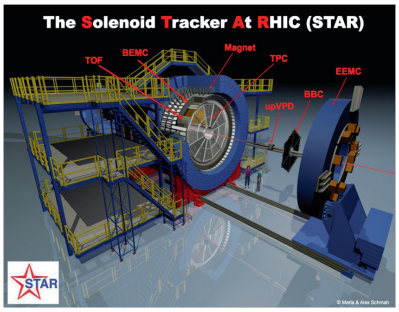

Time of Flight Detector (TOF)

- Timing resolution <100 ps
- Particle identification via 1/β
- Together with TPC provides a good separation of electrons from hadrons up to about 1.5 GeV/c

Barrel Electromagnetic Calorimeter (BEMC)

- Tower Δη×Δφ = 0.05×0.05
- Electron-hadron separation using p/E at high momentum

Data Analysis

Data used are 377M minimum bias U+U collisions at $\sqrt{s_{NN}}$ = 193 GeV taken in 2012.
Electrons are selected from good quality tracks with |η|<1 using TPC, TOF and BEMC:

TPC

- nσ - distance from the expected mean value of the energy loss expressed as number of standard deviations
- -1.5 < nσ electron < 2

TOF

- 0.97 < 1/β < 1.025
- Used: • p < 1.4 GeV/c — strictly required
  • p > 1.4 GeV/c — only if the particle has a TOF signal

BEMC

- Used only for p > 1.4 GeV/c
- 0.5 < pc/E < 2.0

Reconstruction efficiency is obtained from data and MC simulation

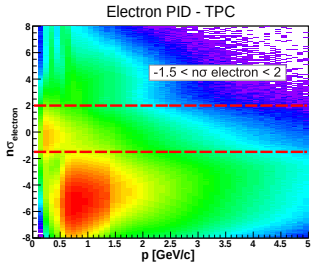

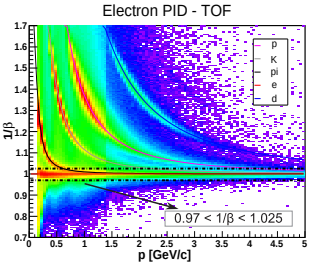

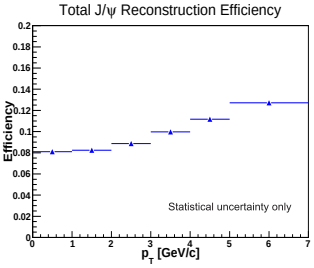

Results

- J/ψ → e^+e^- channel used for the analysis (branching ratio 5.9%)
- Combinatorial background reconstruction: Like-sign method ($e^+e^+ + e^-e^-$ pairs)
- Signal significance calculated in mass region (2.9 - 3.2) GeV/c^2 as

$$sg = \frac{S}{\sqrt{S+2B}}$$

- S = 10900 ± 1300 with significance 11 σ
- Signal divided into 6 p_T bins from 0 to 7 GeV/c
- Nuclear modification factor R_{AA}:

$$R_{AA} = \frac{\sigma^{inel}_{pp}}{< N_{coll} >} \frac{d^2 N_{AA} / dy\, dp_T}{d^2 \sigma_{pp} / dy\, dp_T}$$

is similar as that in Au+Au collisions

- p+p data from collisions at 200 GeV used as the baseline:

STAR [2]	p_T > 2 GeV/c
PHENIX [7]	p_T < 2 GeV/c

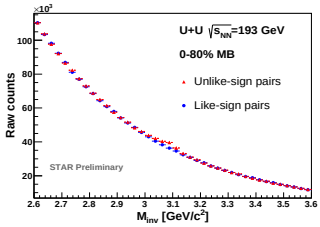

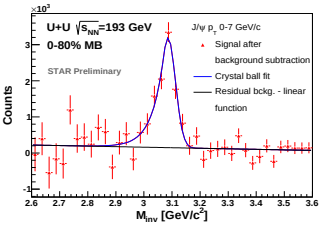

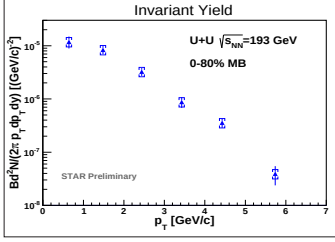

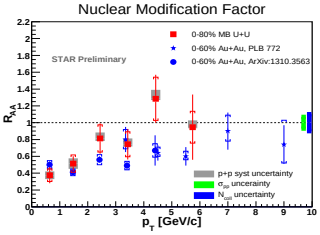

Conclusions and Perspectives

- J/ψ signal of significance of 11 σ (p_T 0-7 GeV/c) observed in U+U collisions at $\sqrt{s_{NN}}$ = 193 GeV
- First STAR measurement of J/ψ nuclear modification factor in U+U presented
- Nuclear modification factor as a function of p_T is similar as in Au+Au collisions

References

[1] D. Kikola et al., Phys.Rev. C84,054907 (2011)
[2] L. Adamczyk et al. [STAR Collaboration], Phys. Lett. B722, 55-62 (2013)
[3] L. Adamczyk et al. [STAR Collaboration], ArXiv 1310.3563 (2013)
[4] Y. Liu et al., Phys. Lett B678, 72 (2009)
[5] X. Zhao and R. Rapp, Phys. Rev. C82, 064905 (2010)
[6] G. Wang, Nuclear Physics A904–905, 248c-255c (2013)
[7] A.Adare et al. [PHENIX Collaboration], PhysRevD.82, 012001 (2010)

Acknowledgement: This work was supported by the grant of the Grant Agency of Czech Republic n. 13-20841S and by the Grant Agency of the Czech Technical University in Prague, grant No. SGS13/215OHK4/3T/14.

* kukral@rcf.rhic.bnl.gov.

Presented at the Quark Matter 2014, Darmstadt, Germany, 19-24 May, 2014